Ore Geology Reviews 149 (2022) 105117

Contents lists available at ScienceDirect

Ore Geology Reviews

journal homepage: www.elsevier.com/locate/oregeorev

Geochemical prospecting of polymetallic mineralization in Gimbi-Nejo area, West Ethiopia

KHAN Junaid [a,b], Hua-Zhou Yao [a,b,*], Kai-Xu Chen [b], Jing-Yin Xu [c], Jian-Xiong Wang [b], Wei-Guo Sun [c], TAHIR Asma [a,b], Yan-Guang Wei [d], Fang Song [b]

[a] School of Earth Sciences, Institute of Geological Survey, China University of Geosciences, Wuhan 430074, China
[b] China Geological Survey, Wuhan Center 430205, Hubei, China
[c] Geophysical Exploration Brigade of Hubei Geological Bureau, Wuhan 430056, Hubei, China
[d] China Geological Survey, Beijing 100037, China

ARTICLE INFO

Keywords:
Geochemical exploration
Stream sediment samples
Geological features
Elements
Economic minerals

ABSTRACT

It is strongly believed that tremendous resources of precious metals and oxides are hidden in the West Ethiopian region. The present work presents a significant test to conduct oriented geochemical mapping for forty-two elements combined with typical geological features in the Pan-African basement exposed area using stream sediment and rock samples. The stream sediments most likely contain some elements directly derived from the surrounding Precambrian to Tertiary bedded metamorphic and igneous intrusive rock units. The obtained data suggest high economic potentials for Au (2.14 ng/g), Cu (43.56 μg/g), Cr (365.1 μg/g), Ni (69.2 μg/g), Co (34.46 μg/g), V (204.1 μg/g), Ti (13278 μg/g), Mn (1472 μg/g), Fe_2O_3 (10.97 %), P (888 μg/g), Al_2O_3 (14.05 %), Ba (501.7 μg/g), Zr (309.5 μg/g), Sr (155.7 μg/g), and Nb (28.2 μg/g). In the composite geochemical anomalies maps, anomalous zones HS12, HS16, HS18, HS19, HS20, and HS28 suggest that transitional metals of intense differentiation with high average contents as compared to Chinese recommended values may be the favourable focus of exploration in the migmatitic gneiss (Cu ~ 66.38 μg/g), granitic orthogneiss (Zr ~ 426.9 μg/g), upper basalt/lower basalt (Nb ~ 63.4 μg/g), meta-volcanic (Mn ~ 2680 μg/g, Ti ~ 29823 μg/g, V ~ 365.6 μg/g, Fe_2O_3 ~ 1629 %), meta-sedimentary formation (Au ~ 5.3 ng/g), Abshala tectonic melange (Cr ~ 2457.1 μg/g), and meta-ultrabasic rocks (Co ~ 62.65 μg/g, Cu ~ 66.38 μg/g, Ni ~ 313.4 μg/g). In conclusion, fifteen ore-forming elements are distinctively abnormal in the area with sixty-four new discovered mineralized spots.

1. Introduction

Stream sediments, especially their geochemistry, may indicate their source lithology (Young et al., 2013; Kirkwood et al., 2016), thus making them a strategic exploration tool (Fletcher, 1997). Stream sediment-based prospecting is commonly useful in areas with various drainage system (Nforba et al., 2020). Geochemical mapping has been effectively used to describe significant mineralization in the region of high to low relief, and in complicated geological settings (Chandrajith et al., 2001). In many countries, this type of work is commonly utilized based on a variety of medium, such as stream sediments, soils, rocks, etc. (Darnley, 1990; Reimann et al., 1998; Rice, 1999; Key et al., 2004; Salminen et al., 2005).

Literature reviews show that both basic geology and mineral resources in Ethiopia are relatively not extensively investigated. The general reviews of Ethiopian industrial minerals were published only before the 21st century by Hamrla (1978), Knot and Abera (1983), Sabov et al. (1983), Getaneh and Saxena (1984), Getaneh (1985), Mengistu (1987), Mengistu and Fentaw (1993, 1994, 2000), Abera (1994), Fentaw and Mengistu (1998), and Fentaw and Mohammed (1999). The Ethiopian crystalline basements contain almost all well-known mineral commodities of the country (Tadesse et al., 2003). A new metallogenic province of epithermal-type gold mineralization has been recently discovered in the Ethiopian rift zone (Tadesse, 2000, 2001). Most of gold deposits in north and south Ethiopia have been successively studied by Billay et al. (1997), Deksissa and Koeberl (2002, 2004), and Tadesse (2004). Similarly, nickel and cobalt deposits in southern Ethiopia have also investigated by Goossens (2000), and Selassie and Reimold (2000). Geological terrains can be evaluated by a stream sediment survey (Ranasinghe et al., 2009), allowing discovery of

* Corresponding author at: School of Earth Sciences, Institute of Geological Survey, China University of Geosciences, Wuhan 430074, China.
E-mail addresses: ycxc2009@126.com, junaidkhan5615@yahoo.com (H.-Z. Yao).

https://doi.org/10.1016/j.oregeorev.2022.105117
Received 9 September 2021; Received in revised form 19 September 2022; Accepted 19 September 2022
Available online 21 September 2022

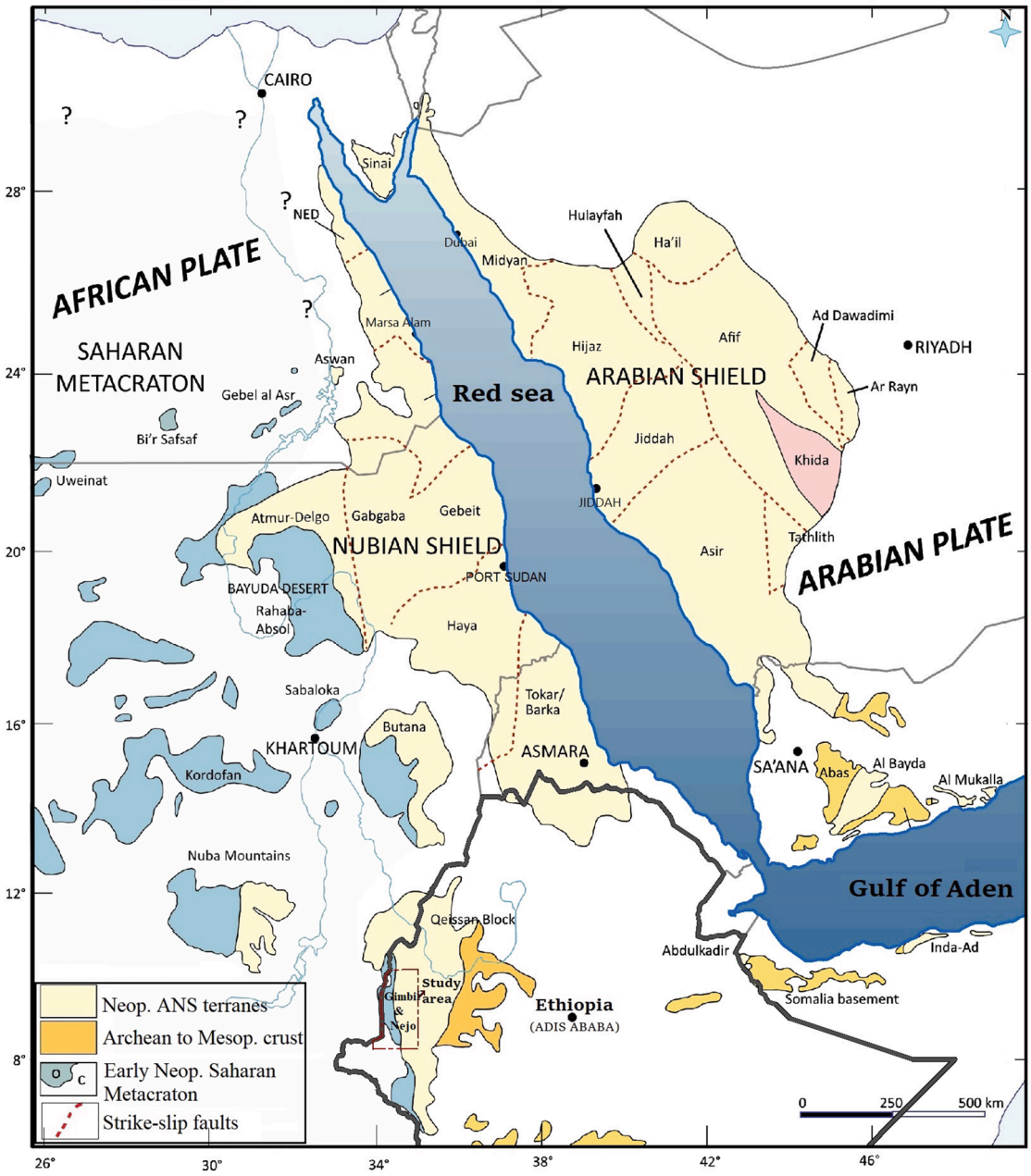

Fig. 1. The tectonic map of the Arabian-Nubian Shield shows the project area's location, Gimbi-Nejo west Ethiopia (modified after Stern et al., 2005; Woldemichael et al., 2009; Johnson et al., 2011; Ghebretensae et al., 2019).

ore deposits. The western Ethiopia ultramafic complexes are associated with enrichments in platinum-group elements (Belete et al., 2000; Selassie and Reimold, 2000). According to Getaneh (1985), radioactive minerals are primarily deposited in Precambrian granites, Cretaceous, and Jurassic sediments of eastern Ethiopia. The geochemical data are used for different purposes such as mineral exploration, agricultural land management, environmental monitoring, etc. (Appleton and Ridgway, 1992; Plant et al., 2001). The geological setting of the Gimbi-Nejo area in west Ethiopia shows the high potential of economic minerals, but no comprehensive efforts have been made to evaluate the regional mineral potential due to warfare and the lack of transportation routes. The main aim of this regional multi-element geochemical prospecting is to use stream sediment and rock samples to explore the following: high potential ore-forming elements, new economic sites of mineralization associated with geological features, and anomalous zones for the focus of mineral exploration from multi-element geochemical mapping in the Gimbi-Nejo area, West Ethiopia.

2. Study area

Gimbi-Nejo (9100 km^2) is located in the western plateau of Ethiopia, between latitudes 9°00′ to 10°00′ N and longitudes 35°15′ to 36°00′ E (Fig. 1). Due to predominantly tropical highland and subtropical forest in the working area, the outcrops are in fair condition with various degrees of weathering. The stream sediments are the product of deposition of weathered rocks/minerals.

2.1. Geological setting

Gimbi-Nejo is considered the most representative exposed area of the Pan-African basements in west Ethiopia. Many previous works, such as Kazmin (1971, 1975) Kazmin et al. (1978), Gass (1981), Kroner (1985),

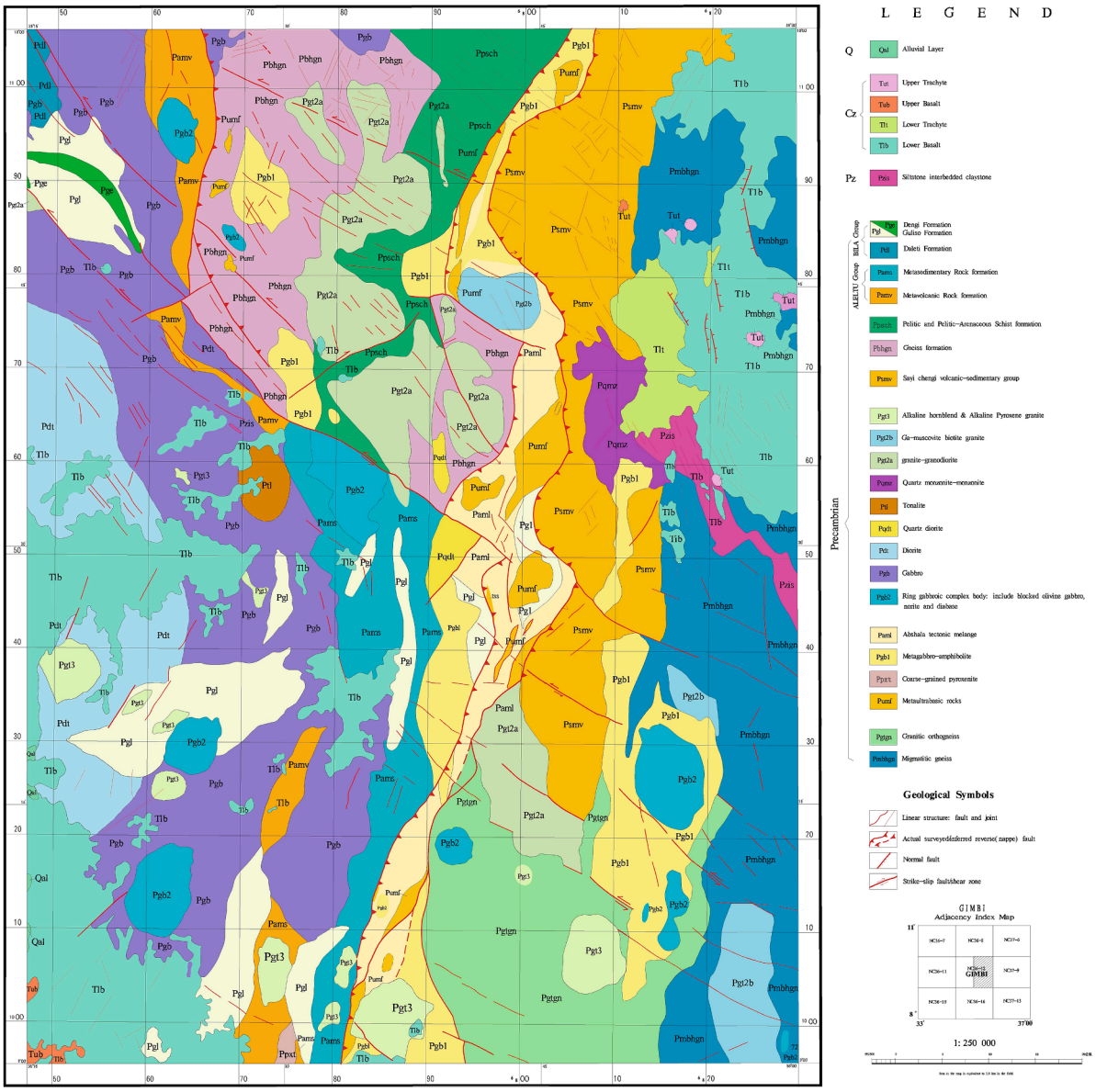

Fig. 2. Geological map of the Gimbi-Nejo area, West Ethiopia.

Kroner et al. (1991), Shackleton (1986, 1994), Stern (1994), Ayalew and Peccerillo (1998), Woldemichael et al. (2009), Williams (2016), and, KHAN et al. (2022), suggest that west Ethiopia had experienced different stages of tectonic activities, which produced unique material records, deformation features, magmatism, and metamorphism. These geological settings indicate high ore potential. Several types of deposits are formed by different geological activities such as crystallization of magma, metamorphism, and weathering, etc. (Arndt et al., 2017).

The study area mainly consists of bedded metamorphic rocks with intrusive and extrusive igneous rock units ranging from the Precambrian to Tertiary. The field survey in combination with literature review (e.g., Kazmin, 1971, 1975; Kazmin et al., 1978; Asrat et al., 2001; Williams, 2016; etc.) shows that Precambrian bedded metamorphic rocks, Paleozoic-Mesozoic sedimentary rocks, Tertiary volcanic rocks, Quaternary deposits, and Tulu Dimtu Tectonic mélange belt are well exposed. The bedded metamorphic rock and stratum comprised various gneisses, pyroclastic and metasedimentary, and meta mafic–ultramafic intrusive rocks that make up about 85 % of the base area. The intrusive rocks are also widely distributed. They vary from basic intrusive rocks, intermediate basic intrusive rocks to intermediate acid intrusive rocks. All these western Ethiopian rock units have a good potential for mineralization (Belete et al., 2000; Mogessie and Belete, 2000; Tadesse et al., 2003). After a field survey based on different deformation patterns, metamorphism, volcanism, and sedimentation, the exposed rock units mentioned above are reclassified on a geological map for understanding the geological features related to mineralization (Fig. 2).

2.2. Drainage system

The stream system is relatively developed in the study area, particularly in Blue Nile and Baro. Regionally, rainfall is strong, but a few areas occasionally lack streams during the dry season. The lineation of most drainage patterns suggests that they are structurally controlled (Fig. 3a). The stream is filled with angular to sub-rounded rock fragments, ranging from boulder to sand in size, while the fine sand, silt, and clay particles are interspersed in the debris.

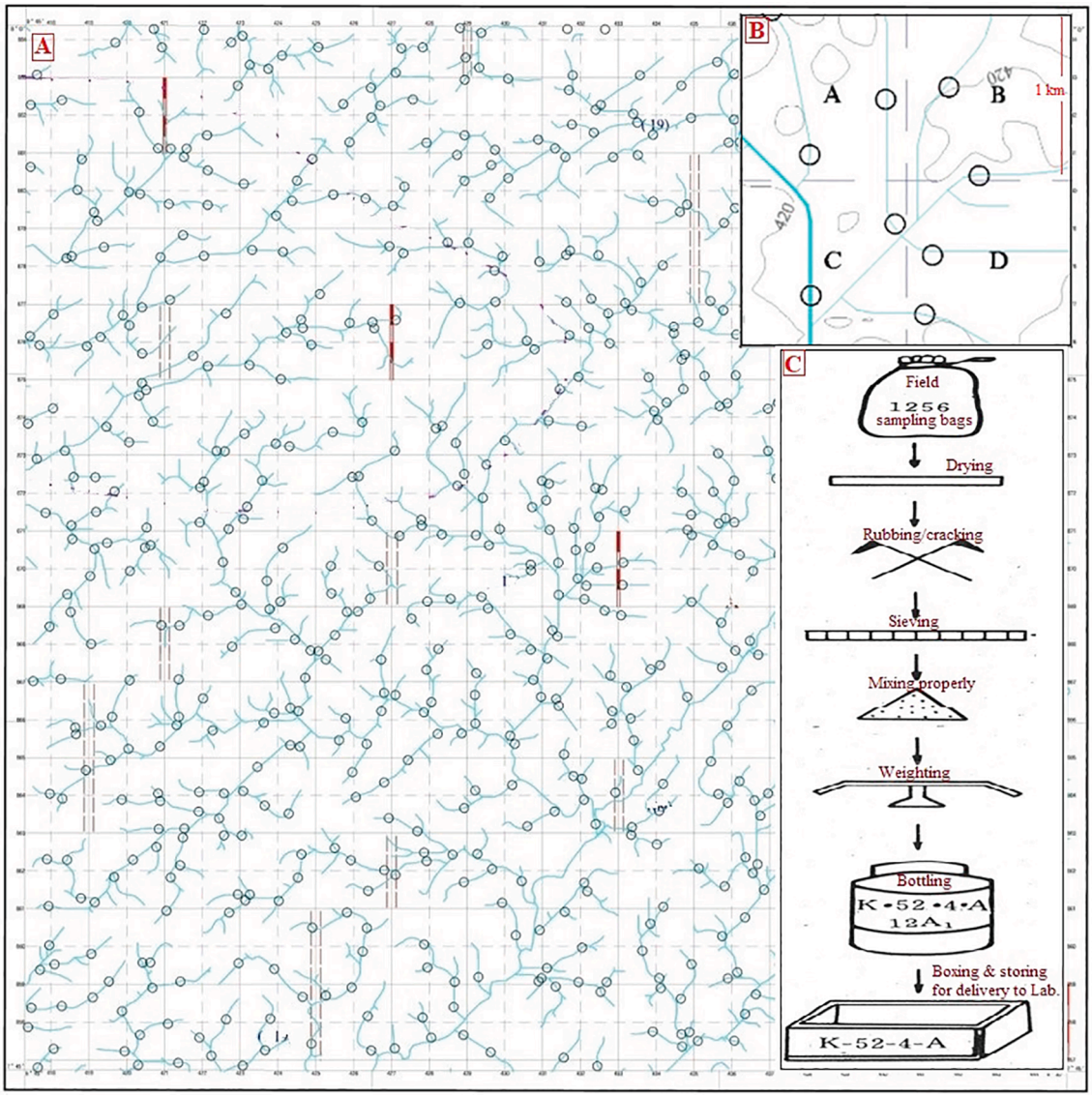

Fig. 3. (A) Sample collection points are evenly distributed on the topographic map.(B) Each big grid cell is divided into four small sampling cell (C) Steps of working procedure after collecting samples in the field camps. Circles are sample points, blue lines are streams, and red dotted lines are drill sampling sites. (For interpretation of the references to colour in this figure legend, the reader is referred to the web version of this article.)

3. Methodology

The 1:250,000 scale geochemical survey in Gimbi-Nejo includes both outdoor work (field sampling) and in-door work (laboratory analysis). The outdoor work mainly involved sampling stream sediments from active drainage systems and rock samples from surrounding outcrops (Ridgway et al., 2009). Multi-methods and multi-instruments were adopted, following the procedure proposed by Cheng et al. (2014) during laboratory work.

3.1. Field sampling procedure (Out-door work)

The field sampling was limited between September and December. The stream sediment samples were collected to detect geochemical signatures related to mineralization, while the rock sampling aimed to measure the trace element composition of the major geological units. This helped to determine the background and relative anomalous levels of the relevant elements in the stream sediment samples. The stream sediments, mainly sludge, siltstone, and sandstone at each site were collected from several points to produce −20 mesh representative composite samples. These samples were mainly collected with a trenching tool from first and second-order streams of 1 km long (Fig. 3). A total of 2254 composite samples weighing 220 g each were collected during the field work. The average sampling density is 2.33 samples per 4 km^2(Fig. 3b). Similarly, 516 rock samples from surrounding outcrops weighing 300 g each were also collected during the field survey. Rock sampling sites were selected based on the lithological variation. The soil samples from undeveloped stream areas and different exploration methods like drill hole testing, trenches, etc., were also adopted to improve the accuracy.

After collection, samples were put into cloth bags with identifying numbers and then taken to the field camp for drying and sieving. Each sieved sample was homogenized, coned, and sub-sampled into two parts in the next step. One part weighing about 100 g was left in bottles for future reference, while the other 120 g was used for further analytical analysis (Fig. 3c). The GPS (eTrex, XL-12) coordinates (UTMzone.36) of each sample position were also recorded for future reference. Quality control during sample collection was to avoid contamination and deterioration (Johnson et al., 2018; Ridgway et al., 2009; Lapworth et al., 2012).

Table 1
Showing the analytical methods with threshold and standard limit of each ore-forming elements.

Elements	Methods	Threshold limit (μg/g)	Standard limit (μg/g)
Ag	ES	0.1	0.02
As	AFS	9.0	1
Au	FAES	0.0035	0.0003
B	ES	32.5	5
Ba	ICP-AES	760	50
Be	ICP-MS	2.15	0.5
Bi	AFS	0.25	0.1
Cd	ICP-MS	0.1	0.03
Co	ICP-MS	60	1
Cr	XRF	500	15
Cu	XRF	70	1
F	ISE	394	100
Hg	AFS	0.025	0.0005
La	ICP-MS	35.9	30
Li	ICP-MS	19.8	5
Mn	ICP-AES	2253	30
Mo	ICP-MS	2.0	0.4
Nb	XRF	42.5	5
Ni	ICP-MS	100	2
P	XRF	1412	100
Pb	ICP-MS	16	2
Pd	FAES	0.0025	0.0003
Pt	FAES	0.0015	0.0003
Rb	XRF	63.6	–
Sb	AFS	0.4	0.1
Sn	ES	3.0	1
Sr	ICP-AES	247	5
Th	ICP-MS	7.7	4
Ti	XRF	25,000	100
U	ICP-MS	3.2	0.5
V	ICP-AES	335	20
W	ICP-MS	2.5	0.5
Y	XRF	38.7	5
Zn	XRF	95	10
Zr	XRF	550	10
SiO_2	XRF	755,000	0.1
Al_2O_3	XRF	197,000	0.05
Fe_2O_3	XRF	188,000	0.05
MgO	ICP-AES	28,800	0.05
CaO	ICP-AES	35,000	0.05
Na_2O	ICP-AES	19,000	0.05
K_2O	XRF	28,000	0.05

Remark: Inductively coupled plasma-atomic emission spectrometry (ICP-AES), X-ray fluorescence spectrum (XRF), inductively coupled plasma mass spectrometry (ICP-MS), Atomic emission spectrometry (ES), Atomic fluorescence spectrometry (AFS), Ionic selection electrometry (ISE), Fire-assay emission spectrography (FAES).

3.2. Sample preparation and analyses (In-door work)

Analysis of soil, composite sediment, and rock samples were conducted in the Test and Monitoring Center of Wuhan (Geochemical Laboratory of China Geological Survey, CGS), the Ministry of Land and Resources China, and also in ALS Chemex (Guangzhou) Co., Ltd, China. All samples were analyzed for 42 selected elements: Cu, Pb, Cd, La, Li, Sn, Fe_2O_3, Mn, Co, P, U, Zr, Th, Rb, Nb, Sr, Ba, Pt, Pd, K_2O, Na_2O, CaO, MgO, V, Mo, Hg, Ni, Cr, Ti, W, Bi, Au, Sb, As, B, SiO_2, Al_2O_3, Y, F, Be, Ag, Zn. A multi-method and multi-instrument analytical approach was adopted (Table 1). Analytical instruments include XRF, ICP-AES, and ICP-MS, and futher analytical techniques were used to evaluate elements with low crustal abundance. All samples including sediments, soil, and rock preparation were completed at the geochemical laboratories; before the samples were analyzed, about 80 g of each sample was dried at 110 °C in the oven then pulverized with a planetary ball mill to 0.074 mm (200 mesh) for the major and trace element analyses, rest sample for future reference.

An automated PANalytical Axios max XRF was used for above element analyses after 400 mg of each sample were pelletized. For the detailed method description of XRF, refer to Beckhoff et al. (2006) . A Thermo X Series-2 VG Elemental ICP-MS was used for element analyses; 250 mg of each sample was dissolved with a mixture of HF + HNO_3 + $HClO_4$ + aqua regia by evaporating to dryness. In a 25 ml (5 %) aqua regia solution, the residue was dissolved. After pipetting, the clear upper solution was 10 ml diluted with HNO_3(2 %). The same procedure with a mixture of HF + HCl + HNO_3 + H_2SO_4 was used to analyze La. For the detailed preparation and analytical method description of ICP-MS, follow Briggs (2002) and Yao et al. (2011). An ICP-AES was used for element analyses; 250 mg of each sample was dissolved with a mixture of HF + HNO_3 + $HClO_4$ + aqua regia by evaporating to dryness. In a 25 ml (3 %) aqua regia solution, the residue was dissolved. The detailed method description of ICP-AES, can be found in Thomas and William (1997), Briggs (2002), Yao et al. (2011) and HU and YI (2017). The detailed method description of further analytical techniques AFS (2202E), ES, ISE, and FAES, are referred to Ficklin (1970), Whitehead & Heady (1970), Cooley et al. (1976), Kuznetsova et al. (2007), Sánchez-Rodas et al. (2010), Yao et al. (2011), Xiong et al. (2011).

China Geological survey set the standard limit for each element (SPC, 2004). The average content of each element was accepted after a 12-time repetition of each analytical process. The histogram of each exposed rock unit and number of Chinese standard reference samples for calibration during each analytical process with detection limit, percent of reported samples, and relative standard deviations (RSD) is present on each element's geochemical anomaly map. The element Au, Pt, and Pd were treated separately with China national geochemical standard reference samples: GBW-07288, GBW-07289, GBW-07290, GBW-07291, GBW-07292, and GBW-07293. The analytical methods with the threshold limit and standard limit of each ore-forming elements are shown in Table 1.

3.3. Quality control

The rigorous analytical quality control procedures were applied using Chinese standard reference samples and duplicate samples (both field and laboratory duplicate samples) to test the precision and accuracy of the methods (Johnson et al., 2005, 2018; Lapworth et al., 2012). A quality control (QC) program covered all features of the geochemical study, from collecting samples in the field to laboratory data analysis. The external quality control was conducted by the inspection unit of a regional geochemical sample analysis quality, China geological survey (CGS) at the end of each workday; field records were rechecked at the field camp to verify that every procedure was done correctly and samples were correctly handled until they were dispatched for laboratory analysis. The sample-site/field duplicate samples were randomly inserted into each batch of 10 samples, subsequently packed into cardboard boxes, and sent to the analytical laboratory in China.

During internal quality control, China national reference samples were simultaneously analyzed in the analytical blocks to appraise the accuracy of the methods. Twelve China national geochemical standard reference samples were inserted into each batch of 500 stream sediment samples. After analysis, the Logarithmic difference ($\triangle$lgC=|lgCi-lgCs|) between measured and standard values was acceptable. In order to control the long-term stability of the methods, four monitoring samples (China national geochemical standard reference samples) were inserted into each batch of 50 stream sediment samples and were regularly analyzed. After analysis, the average log difference of the concentrations (ΔlgC) and the standard deviation (λ (GRD)) was found to be within acceptable standards for all elements. To check the reproducibility of the results statistically, replicate analysis was performed on 5 % of the total number of samples. After analysis, the relative difference (RD = 2×|A1-A2|/|A1 + A2|×100 %) between basic and replicate analysis was also within the acceptable range for each element. The sample-site/field and laboratory duplicate samples were also analyzed to monitor the precision of the analytical methods and sampling error. One hundred nineteen duplicates were collected from the study area and analyzed with the

Table 2
The degree of elemental differentiation in the Gimbi-Nejo area, west Ethiopia.

Differentiation degree	Uniform distribution	Relatively uniform distribution	Differentiation	Strong differentiation
CV interval	<0.5	0.5~0.7	0.7~1.0	≥1.0
Elements	SiO_2, Al_2O_3, Y, F, Be, Ag, Zn	Cu, Pb, Cd, La, Li, Sn, Fe_2O_3, Mn, Co, P, U	Zr, Th, Rb, Nb, Sr, Ba, Pt, Pd, K_2O, Na_2O, CaO, MgO, V, Mo, Hg	Ni, Cr, Ti, W, Bi, Au, Sb, As, B

Table 3
A geochemical anomalous zones contain ore-forming elements associated with geological features of the area.

Name	Elements/ Anomalies	Geological category	Name	Elements/ Anomalies	Geological category
HS1	Cu, Zn, Cd, V	I,V	HS17	Cu, Cr, Ni, Co, V	VI
HS2	W, Bi	III,V	HS18	Au, Ag, Cu, Ni, Sn, Mo	V,VI
HS3	Zn, V, Fe, Ni	II	HS19	Au, Cu, Pt, Pd	III
HS4	Pb, Mo, Sn, Bi	IV	HS20	Au, Pt, Pd, Cu, Ni	II,III
HS5	Cu, Ni, Pt, Pd	II	HS21	Au, As, Sb	III
HS6	Au, Pt, Pd, Cu, Ni	II,III	HS22	Ag, Hg, Ti	V
HS7	Au, Pt, Pd, Cu	I	HS23	Au, Pt, Pd	III,V
HS8	Zn, Cd	I	HS24	Au, Pt, Pd	II,III
HS9	W, Bi	I	HS25	Au, Pt, Pd, Cu, Ni	I
HS10	Au, Ag, W, Bi	III	HS26	Cu, Zn, Ni, Co, V	II
HS11	Au	V	HS27	Ag, Zn, Cd, Ti	V
HS12	Au, Pt, Pd, Cu	I	HS28	Cr, Ni, Co, Ag, Zn, Cd	II
HS13	Pb, W, Bi	IV	HS29	Pt, Pd	II
HS14	Ag, Pb, Mo, Zn	VI	HS30	Ag, Pb, W, Sn, Bi, Mo	V
HS15	Au, Ag, Mo, Bi	IV	HS31	Ag, Pb, Zn, Ni, Sn, Mo	VI
HS16	Au, Pt, Pd, Cu, Cr, Ni	II	HS32	Au, Ag, Zn, Pt, As, Sb	II,III,IV

HS; Geochemical anomalous zone.

normal samples. Assay results of the duplicate samples were checked by plotting the absolute difference between the duplicates against the mean of the duplicates to calculate the relative error (RE% =|A1-A2|/ (A1 + A2) * 100 %). It was also found that no significant differences existed between the analyses of the duplicate pairs, indicating good precision and accuracy levels. A relative error of RE% ≤ 33.3 % was obtained which is negligible. In short, stream sediment samples in the project were consistent with the "standard" requirement, and they are reliable for geochemical mapping and interpretation (Ye, 2002; Xie et al., 2003; Ye and Yao, 2004).

4. Results

4.1. Analytical data

The trace-element concentrations of stream sediment samples are listed in Table 4. These data clearly suggest that about 15 elements have high economic potential with higher contents: Au (2.14 ng/g), Cu (43.56 μg/g), Cr (365.1 μg/g), Ni (69.2 μg/g), Co (34.46 μg/g), V (204.1 μg/g), Ti (13278 μg/g), Mn (1472 μg/g), Fe_2O_3 (10.97 %), P (888 μg/g), Al_2O_3(14.05 %), Ba (501.7 μg/g), Zr (309.5 μg/g), Sr (155.7 μg/g) and Nb (28.2 μg/g). Results of rock samples shown in Table 5 are considered as background values of stream sediments.

4.2. Map compilation

According to elemental concentrations, geochemical anomaly maps of 42 elements and five composite geochemical anomaly maps were acquired using the MAPGIS 6.5 and GeoExpl 2005 softwares from a scanned copy of the topographic sheet NC36-8 (Gimbi) for data manipulation visualization and presentation (Figs. 4 & 5). The regional geological map was also generated to link anomalous levels of elements and geological units. Anomalous contours of elements suggest that in the study area, transitional metals enriched with high average contents relative to Chinese recommended values may be the focus of exploration in the migmatitic gneiss (Cu ~ 66.38 μg/g), granitic orthogneiss (Zr ~ 426.9 μg/g), upper basalt/lower basalt (Nb ~ 63.4 μg/g), meta-volcanic (Mn ~ 2680 μg/g, Ti ~ 29823 μg/g, V ~ 365.6 μg/g, Fe_2O_3 ~ 16290000 μg/g), meta-sedimentary formation (Au ~ 0.0053 μg/g), Abshala tectonic melange (Cr ~ 2457.1 μg/g), and meta-ultrabasic rocks (Co ~ 62.65 μg/g, Cu ~ 66.38 g/g, Ni ~ 313.4 μg/g). Consequently, it is interesting to establish 64 newly mineralized sites (31 Au, 16 Cu, 10 Ni

Table 4
A comparison between the whole area average elemental content of stream sediments and Chinese background content of stream sediments.

Elements	Whole area average content	Chinese background content	Percentile	Elements	Whole area average content	Chinese background content	Percentile
Ti	13,278	4155	100	Al_2O_3	14.05	12.98	48.70
Mn	1472	679	97.50	Hg	14	46	46.30
P	888	614	95.10	Li	13.02	32.7	43.90
Ba	501.7	499	92.60	TFe_2O_3	10.97	4.44	41.40
Cr	365.1	58.5	90.20	Pb	10.77	26.0	39.00
Zr	309.5	292	87.80	Th	5.25	11.9	36.50
F	296.6	483	85.30	As	3.66	9.1	34.10
V	204.1	79.7	82.90	Au	2.14	1.3	31.70
Sr	155.7	152	80.40	Sn	2.1	3.4	29.20
Ag	72	80	78.00	U	1.96	2.02	26.80
Cd	71	149	75.60	CaO	1.74	1.77	24.30
Ni	69.2	24.4	73.10	Be	1.538	2.19	21.90
Zn	68.46	68.5	70.70	W	1.5	2.19	17.00
SiO_2	57.28	65.73	68.20	MgO	1.5	1.32	17.00
Cu	43.56	21.6	65.80	Mo	1.366	1.2	12.10
Co	34.46	12.3	60.90	K_2O	1.33	2.35	9.70
Nb	28.2	16.5	58.50	Na_2O	0.98	1.19	4.80
Y	24.5	24.4	56.00	Sb	0.246	0.74	2.40
La	23.17	39.8	53.60	Bi	0.138	0.48	0
B	19.32	42.9	51.20				

Remark: Unit for oxide is "%"; for Au, Ag, Hg, Cd is "ng/g"; & for other is "μg/g".

Table 5
The average content (AC), coefficient of variation and enrichment (CV, CE) of selected elements in each geological rock units of the study area.

Element	Str. sed. of whole area AC	Pgl AC	CE	CV	Pamv AC	CE	CV	Pams AC	CE	CV
Ag	72	81	1.2 ~ 1	0.34	85	1.2 ~ 1	0.492	100	1.5 ~ 1.2	0.316
As	3.66	7.02	>1.8	1.532	3.37	1 ~ 0.8	1.241	11.99	>1.8	0.852
B	19.32	37.62	>1.8	0.802	26.11	1.5 ~ 1.2	0.641	44.41	>1.8	0.501
Ba	501.7	390.2	0.8 ~ 0.5	0.525	356.6	0.8 ~ 0.5	0.53	465.3	1 ~ 0.8	1.094
Be	1.538	1.465	0.8 ~ 0.5	0.431	1.056	0.8 ~ 0.5	0.419	1.49	1 ~ 0.8	0.351
Bi	0.138	0.12	1 ~ 0.8	1.203	0.17	1.5 ~ 1.2	2.537	0.153	1.2 ~ 1	1.46
Cd	71	91	1.5 ~ 1.2	0.759	92	1.5 ~ 1.2	0.554	92	1.5 ~ 1.2	0.528
Co	34.46	36.03	1.2 ~ 1	0.579	47.58	1.5 ~ 1.2	0.301	39.88	1.2 ~ 1	0.451
Cr	365.1	399.7	1.2 ~ 1	4.71	200.5	0.8 ~ 0.5	0.508	262.1	0.8 ~ 0.5	1.114
Cu	43.56	54.09	1.5 ~ 1.2	0.47	58.29	1.5 ~ 1.2	0.389	55.84	1.5 ~ 1.2	0.467
F	296.6	268.2	1 ~ 0.8	0.324	281.1	1 ~ 0.8	0.248	297.7	1.2 ~ 1	0.295
Hg	14	19	1.5 ~ 1.2	0.552	12	1 ~ 0.8	0.779	17	1.5 ~ 1.2	0.385
La	23.17	21.79	1 ~ 0.8	0.389	14.59	0.8 ~ 0.5	0.345	22.71	1 ~ 0.8	0.304
Li	13.02	15.39	1.2 ~ 1	0.426	12.47	1 ~ 0.8	0.511	14.08	1.2 ~ 1	0.416
Au	2.14	4.63	>1.8	4.005	2.01	1 ~ 0.8	1.257	5.3	>1.8	0.991
Mn	1472	1398	1 ~ 0.8	0.52	2680	>1.8	0.793	1481	1.2 ~ 1	0.364
Mo	1.366	1.424	1.2 ~ 1	0.563	0.971	0.8 ~ 0.5	0.559	1.481	1.2 ~ 1	0.475
Nb	28.2	21.3	0.8 ~ 0.5	0.53	15.2	0.8 ~ 0.5	0.333	22.1	0.8 ~ 0.5	0.368
Ni	69.2	69.3	1.2 ~ 1	1.561	69	1.2 ~ 1	0.667	69.3	1.2 ~ 1	0.599
P	888	869	1 ~ 0.8	0.374	875	1 ~ 0.8	0.387	819	1 ~ 0.8	0.454
Pb	10.77	9.91	1 ~ 0.8	0.37	6.17	0.8 ~ 0.5	0.375	11.71	1.2 ~ 1	0.351
Pd	1.43	1.66	1.2 ~ 1	1.116	1.99	1.5 ~ 1.2	1.28	1.89	1.5 ~ 1.2	0.624
Pt	1.06	1.09	1.2 ~ 1	0.76	1.18	1.2 ~ 1	1.149	1.32	1.5 ~ 1.2	0.47
Rb	40.98	31.27	0.8 ~ 0.5	0.42	22.31	0.8 ~ 0.5	0.534	35.73	1 ~ 0.8	0.363
Sb	0.246	0.348	1.5 ~ 1.2	0.954	0.245	1.2 ~ 1	0.616	0.533	>1.8	0.508
Sn	2.1	2.05	1 ~ 0.8	0.484	1.6	0.8 ~ 0.5	0.455	2.13	1.2 ~ 1	0.28
Sr	155.7	109	0.8 ~ 0.5	0.684	162.1	1.2 ~ 1	0.493	106.8	0.8 ~ 0.5	0.487
Th	5.25	4.64	1 ~ 0.8	0.386	3.2	0.8 ~ 0.5	0.459	5.36	1.2 ~ 1	0.308
Ti	13,278	12,255	1 ~ 0.8	0.87	29,823	>1.8	1.325	10,465	0.8 ~ 0.5	0.525
U	1.96	1.81	1 ~ 0.8	0.388	1.1	0.8 ~ 0.5	0.515	1.99	1.2 ~ 1	0.295
V	204.1	205.7	1.2 ~ 1	0.384	365.6	1.8 ~ 1.5	0.784	198.4	1 ~ 0.8	0.428
W	1.5	1.75	1.2 ~ 1	0.631	3.04	>1.8	1.297	2.31	1.8 ~ 1.5	1.182
Y	24.5	24.31	1 ~ 0.8	0.269	21.24	1 ~ 0.8	0.225	24.88	1.2 ~ 1	0.298
Zn	68.46	72.33	1.2 ~ 1	0.379	88.63	1.5 ~ 1.2	0.326	70.49	1.2 ~ 1	0.329
Zr	309.5	264	1 ~ 0.8	0.577	168.9	0.8 ~ 0.5	0.418	292.8	1 ~ 0.8	0.582
SiO2	57.28	56.85	1 ~ 0.8	0.185	48.02	1 ~ 0.8	0.252	58.7	1.2 ~ 1	0.174
Al2O3	14.05	14.56	1.2 ~ 1	0.256	14.08	1.2 ~ 1	0.323	13.94	1.2 ~ 1	0.258
Fe2O3	10.97	10.92	1.2 ~ 1	0.392	16.29	1.5 ~ 1.2	0.569	10.52	1 ~ 0.8	0.375
MgO	1.5	1.29	1 ~ 0.8	1.063	2.64	1.8 ~ 1.5	0.454	1.06	0.8 ~ 0.5	0.505
CaO	1.74	1.24	0.8 ~ 0.5	0.992	2.96	1.8 ~ 1.5	0.505	0.93	0.8 ~ 0.5	0.646
Na2O	0.98	0.58	0.8 ~ 0.5	0.789	0.95	1 ~ 0.8	0.671	0.72	0.8 ~ 0.5	0.632
K2O	1.33	0.93	0.8 ~ 0.5	0.472	0.64	<0.5	0.75	1.12	1 ~ 0.8	0.473

	Ppsch			Pbhgn			Psmv	
AC	CE	CV	AC	CE	CV	AC	CE	CV
66	1 ~ 0.8	0.38	59	1 ~ 0.8	0.435	70	1 ~ 0.8	0.503
3.82	1.2 ~ 1	1.399	1.24	<0.5	1.038	7.76	>1.8	1.11
26.57	1.5 ~ 1.2	1.032	10.45	1.5 ~ 1.2	1.266	28.9	1.8 ~ 1.5	1.761
837.7	1.8 ~ 1.5	0.441	595.2	0.8 ~ 0.5	0.801	453.5	1 ~ 0.8	0.375
1.695	1.2 ~ 1	0.417	1.351	1 ~ 0.8	0.345	1.394	1 ~ 0.8	0.296
0.434	>1.8	2.964	0.282	>1.8	3.123	0.132	1 ~ 0.8	0.767
67	1 ~ 0.8	0.507	68	1 ~ 0.8	0.578	77	1.2 ~ 1	0.468
17.39	0.8 ~ 0.5	0.618	22.46	0.8 ~ 0.5	0.658	38.47	1.2 ~ 1	0.578
112.5	<0.5	0.877	101.7	<0.5	1.221	698.3	>1.8	2.226
29.86	0.8 ~ 0.5	0.56	29.63	0.8 ~ 0.5	0.657	48.9	1.2 ~ 1	0.501
344.3	1.2 ~ 1	0.358	303.9	1.2 ~ 1	0.455	326.3	1.2 ~ 1	0.282
6	<0.5	0.837	9	0.8 ~ 0.5	0.798	10	0.8 ~ 0.5	0.652
15.31	0.8 ~ 0.5	0.403	16.19	0.8 ~ 0.5	0.645	18.09	0.8 ~ 0.5	0.341
16.09	1.5 ~ 1.2	0.481	11.85	1 ~ 0.8	0.539	11.32	1 ~ 0.8	0.426
0.96	<0.5	1.037	1.43	0.8 ~ 0.5	1.45	3.07	1.5 ~ 1.2	1.641
1068	0.8 ~ 0.5	0.504	1137	0.8 ~ 0.5	0.648	1490	1.2 ~ 1	0.631
1.077	0.8 ~ 0.5	0.481	0.874	0.8 ~ 0.5	0.529	1.24	1 ~ 0.8	0.401
24.4	1 ~ 0.8	1.334	16.2	0.8 ~ 0.5	0.485	22.5	1 ~ 0.8	0.626
32.3	<0.5	0.671	36.8	0.8 ~ 0.5	1.02	107.3	1.8 ~ 1.5	1.059
524	0.8 ~ 0.5	0.486	688	0.8 ~ 0.5	0.693	714	1 ~ 0.8	0.435
15.22	1.5 ~ 1.2	0.35	10.33	1 ~ 0.8	0.591	8.91	1 ~ 0.8	0.396
0.89	0.8 ~ 0.5	0.675	1.12	1 ~ 0.8	0.884	1.61	1.2 ~ 1	0.915
0.74	0.8 ~ 0.5	1.362	0.92	1 ~ 0.8	0.682	1.14	1.2 ~ 1	0.865
66.01	1.8 ~ 1.5	0.455	49.26	1.5 ~ 1.2	0.739	34.75	1 ~ 0.8	0.476
0.231	1 ~ 0.8	0.823	0.13	0.8 ~ 0.5	0.55	0.387	1.8 ~ 1.5	0.924
1.79	1 ~ 0.8	0.545	1.54	0.8 ~ 0.5	0.484	2.12	1.2 ~ 1	0.424
227.2	1.5 ~ 1.2	0.435	238	1.8 ~ 1.5	0.692	145.3	1 ~ 0.8	0.508
6.71	1.5 ~ 1.2	1.327	3.86	0.8 ~ 0.5	0.402	3.94	0.8 ~ 0.5	0.408

(*continued on next page*)

Table 5 (*continued*)

	Ppsch			Pbhgn			Psmv	
AC	CE	CV	AC	CE	CV	AC	CE	CV
6314	<0.5	0.844	10,673	1 ~ 0.8	1.492	11,065	1 ~ 0.8	0.972
3.08	1.8 ~ 1.5	1.477	1.67	1 ~ 0.8	0.603	1.48	0.8 ~ 0.5	0.412
130.3	0.8 ~ 0.5	0.605	150.5	0.8 ~ 0.5	0.709	189.4	1 ~ 0.8	0.701
2.22	1.5 ~ 1.2	1.117	1.78	1.5 ~ 1.2	1.684	1.61	1.2 ~ 1	0.996
22.66	1 ~ 0.8	0.801	19.69	1 ~ 0.8	0.437	23.37	1 ~ 0.8	0.33
55.19	1 ~ 0.8	0.458	55.96	1 ~ 0.8	0.532	78.87	1.2 ~ 1	0.543
278.3	1 ~ 0.8	1.182	257.8	1 ~ 0.8	0.961	229.7	0.8 ~ 0.5	0.895
66.65	1.2 ~ 1	0.132	64.19	1.2 ~ 1	0.206	58.29	1.2 ~ 1	0.185
12.13	1 ~ 0.8	0.181	12.11	1 ~ 0.8	0.261	12.77	1 ~ 0.8	0.197
6.65	0.8 ~ 0.5	0.475	7.88	0.8 ~ 0.5	0.707	10.81	1 ~ 0.8	0.491
1.45	1 ~ 0.8	0.604	1.74	1.2 ~ 1	0.657	2.29	1.8 ~ 1.5	0.624
1.87	1.2 ~ 1	0.678	2.4	1.5 ~ 1.2	0.619	2.05	1.5 ~ 1.2	0.699
1.44	1.5 ~ 1.2	0.375	1.43	1.5 ~ 1.2	0.469	1.37	1.5 ~ 1.2	0.52
2.26	1.8 ~ 1.5	0.437	1.66	1.5 ~ 1.2	0.711	1.26	1 ~ 0.8	0.597
	Paml			Pumf			Pmbhgn	
AC	CE	CV	AC	CE	CV	AC	CE	CV
78	1.2 ~ 1	0.367	85	1.2 ~ 1	0.483	45	0.8 ~ 0.5	0.525
5.32	1.5 ~ 1.2	1.371	7.68	>1.8	0.974	0.9	<0.5	1.068
33.78	1.8 ~ 1.5	1.605	34.63	1.8 ~ 1.5	0.835	4.24	<0.5	1.065
378.4	0.8 ~ 0.5	0.423	341	0.8 ~ 0.5	0.589	745.5	1.5 ~ 1.2	0.659
1.251	1 ~ 0.8	0.275	1.145	0.8 ~ 0.5	0.391	1.46	1 ~ 0.8	0.374
0.09	0.8 ~ 0.5	1.075	0.084	0.8 ~ 0.5	0.633	0.058	<0.5	0.719
78	1.2 ~ 1	0.493	78	1.2 ~ 1	0.4	52	0.8 ~ 0.5	0.538
49.27	1.5 ~ 1.2	0.804	62.65	>1.8	0.656	17.48	0.8 ~ 0.5	0.764
2457.1	>1.8	4.082	2136.2	>1.8	2.548	95	<0.5	1.564
50.96	1.5 ~ 1.2	0.461	66.38	1.8 ~ 1.5	0.307	23.14	0.8 ~ 0.5	0.747
280.1	1 ~ 0.8	0.235	277.6	1 ~ 0.8	0.207	255.4	1 ~ 0.8	0.38
10	0.8 ~ 0.5	0.558	9	0.8 ~ 0.5	0.695	7	0.8 ~ 0.5	0.655
16.76	0.8 ~ 0.5	0.361	15.43	0.8 ~ 0.5	0.47	17.09	0.8 ~ 0.5	0.698
11.33	1 ~ 0.8	0.471	12.48	1 ~ 0.8	0.387	8.81	0.8 ~ 0.5	0.481
2.6	1.5 ~ 1.2	1.159	2.67	1.5 ~ 1.2	1.118	0.77	<0.5	0.995
1668	1.2 ~ 1	0.427	2098	1.5 ~ 1.2	0.678	890	0.8 ~ 0.5	0.55
0.847	0.8 ~ 0.5	0.504	1.023	0.8 ~ 0.5	0.897	0.877	0.8 ~ 0.5	0.587
20.8	0.8 ~ 0.5	0.424	18.8	0.8 ~ 0.5	0.523	21.5	0.8 ~ 0.5	0.694
206.2	>1.8	1.653	313.4	>1.8	1.909	28.7	<0.5	1.122
662	0.8 ~ 0.5	0.4	726	1 ~ 0.8	0.489	584	0.8 ~ 0.5	0.857
7.44	0.8 ~ 0.5	0.357	6.99	0.8 ~ 0.5	0.61	11.89	1.2 ~ 1	0.383
2.2	1.8 ~ 1.5	1.004	2.04	1.5 ~ 1.2	0.665	1.23	1 ~ 0.8	0.796
1.62	1.8 ~ 1.5	0.972	1.65	1.8 ~ 1.5	1.011	0.95	1 ~ 0.8	0.835
28.34	0.8 ~ 0.5	0.369	22.92	0.8 ~ 0.5	0.488	59.19	1.5 ~ 1.2	0.436
0.268	1.2 ~ 1	1.032	0.451	>1.8	1.246	0.113	<0.5	0.694
2.47	1.5 ~ 1.2	0.964	2.07	1 ~ 0.8	1.29	1.68	1 ~ 0.8	0.329
147.8	1 ~ 0.8	0.433	157.1	1.2 ~ 1	0.507	169	1.2 ~ 1	0.498
4.04	0.8 ~ 0.5	0.525	2.75	0.8 ~ 0.5	0.491	5.05	1 ~ 0.8	0.43
13,336	1.2 ~ 1	0.853	16,091	1.5 ~ 1.2	0.874	6765	0.8 ~ 0.5	0.909
1.36	0.8 ~ 0.5	0.394	0.98	0.8 ~ 0.5	0.489	2.12	1.2 ~ 1	0.453
178.7	1 ~ 0.8	0.39	266	1.5 ~ 1.2	0.536	110.6	0.8 ~ 0.5	0.621
1.46	1 ~ 0.8	0.794	1.22	1 ~ 0.8	0.529	0.71	<0.5	0.551
20.89	1 ~ 0.8	0.265	20.6	1 ~ 0.8	0.233	18.84	0.8 ~ 0.5	0.495
76.14	1.2 ~ 1	0.531	86.21	1.5 ~ 1.2	0.304	47.33	0.8 ~ 0.5	0.526
267	1 ~ 0.8	0.815	160.3	0.8 ~ 0.5	0.54	281.3	1 ~ 0.8	0.964
58.76	1.2 ~ 1	0.182	49.27	1 ~ 0.8	0.117	67.41	1.2 ~ 1	0.153
11.78	1 ~ 0.8	0.222	13.86	1 ~ 0.8	0.165	11.94	1 ~ 0.8	0.233
10.72	1 ~ 0.8	0.394	14.55	1.5 ~ 1.2	0.294	6.3	0.8 ~ 0.5	0.608
2.61	1.8 ~ 1.5	0.724	3.73	>1.8	0.528	1.1	0.8 ~ 0.5	0.838
2.27	1.5 ~ 1.2	0.455	3.15	>1.8	0.625	1.66	1 ~ 0.8	0.684
1.08	1.2 ~ 1	0.501	1.23	1.5 ~ 1.2	0.648	1.6	1.8 ~ 1.5	0.525
0.84	0.8 ~ 0.5	0.449	0.65	<0.5	0.604	2.56	>1.8	0.605
	Pgtgn			Tub/Tib			Pgt3/Pgt2	
AC	CE	CV	AC	CE	CV	AC	CE	CV
73	1.2 ~ 1	0.32	78	1.08	0.46	62	0.86	0.6
1.47	<0.5	0.557	2.96	0.81	0.63	1.89	0.52	1.06
6.82	<0.5	0.453	14.99	0.78	2.04	13.92	0.72	1.89
466.5	1 ~ 0.8	0.546	463	0.92	0.72	753	1.5	0.68
1.628	1.2 ~ 1	0.624	2.24	1.46	0.35	1.79	1.17	0.46
0.113	1 ~ 0.8	0.731	0.1	0.72	0.84	0.23	1.68	1.92
66	1 ~ 0.8	0.504	77	1.08	0.4	55	0.77	0.56
27.58	1 ~ 0.8	0.587	43.29	1.26	0.53	18.63	0.54	0.94
89.2	<0.5	0.833	347.1	0.95	1.5	181.2	0.5	2.82
26.69	0.8 ~ 0.5	0.516	53.5	1.23	0.4	26.2	0.6	0.9
305.9	1.2 ~ 1	0.342	365.3	1.23	0.34	284.7	0.96	0.34
15	1.2 ~ 1	0.497	22	1.55	0.7	12	0.85	0.97

(*continued on next page*)

Table 5 (*continued*)

	Pgtgn			Tub/Tib			Pgt3/Pgt2	
AC	CE	CV	AC	CE	CV	AC	CE	CV
23.93	1.2 ~ 1	0.399	45.41	1.96	0.48	19.28	0.83	0.71
9.23	0.8 ~ 0.5	0.477	18.29	1.4	0.53	13.38	1.03	0.42
1.14	0.8 ~ 0.5	0.776	1.41	0.66	1.21	1.61	0.75	1.4
1380	1 ~ 0.8	0.503	1575	1.07	0.48	977	0.66	0.79
1.17	1 ~ 0.8	0.338	2.67	1.95	0.56	1.27	0.93	0.61
24.3	1 ~ 0.8	0.332	63.4	2.25	0.56	26.5	0.94	1.08
34.4	<0.5	0.853	93.5	1.35	0.59	35.8	0.52	1.3
1012	1.2 ~ 1	0.456	1316	1.48	0.51	630	0.71	0.74
8.18	0.8 ~ 0.5	0.378	13.78	1.28	0.39	16.18	1.5	0.43
1.67	1.2 ~ 1	0.696	1.2	0.84	0.63	1.2	0.83	0.88
1.56	1.5 ~ 1.2	0.921	0.91	0.86	0.62	1.04	0.98	0.79
37.5	1 ~ 0.8	0.51	40.51	0.99	0.54	77.47	1.89	0.57
0.114	<0.5	0.338	0.28	1.14	0.81	0.17	0.68	0.9
2.56	1.5 ~ 1.2	0.372	2.93	1.4	0.41	2.3	1.1	0.65
98.3	0.8 ~ 0.5	0.511	134.1	0.86	0.77	173.8	1.12	0.79
5.99	1.2 ~ 1	0.444	8.05	1.53	0.43	7.13	1.36	1.31
13,312	1.2 ~ 1	0.771	14,868	1.12	0.49	8543	0.64	1.39
2.17	1.2 ~ 1	0.443	2.67	1.36	0.43	2.8	1.43	0.59
148.7	0.8 ~ 0.5	0.485	255.2	1.25	0.41	120.1	0.59	1.06
1.29	1 ~ 0.8	0.425	1.45	0.96	0.65	1.5	1	1.15
25.28	1.2 ~ 1	0.368	35	1.43	0.38	19.95	0.81	0.58
62.61	1 ~ 0.8	0.374	81.22	1.19	0.35	50.48	0.74	0.59
426.9	1.5 ~ 1.2	0.742	395.5	1.28	0.41	297.8	0.96	0.93
61.6	1.2 ~ 1	0.19	46.09	0.8	0.3	66.58	1.16	0.19
12.34	1 ~ 0.8	0.303	18.01	1.28	0.23	12.64	0.9	0.27
8.92	1 ~ 0.8	0.433	15.67	1.43	0.43	6.4	0.58	0.81
1.29	1 ~ 0.8	0.557	1.02	0.68	0.64	0.91	0.61	0.89
1.55	1 ~ 0.8	0.612	1.08	0.62	0.89	1.2	0.69	0.81
0.64	0.8 ~ 0.5	0.549	0.66	0.67	1.25	1.14	1.17	0.63
1.27	1 ~ 0.8	0.586	1.15	0.87	1.14	2.52	1.89	0.58

	Pdt/Pgd			Pgb1/Pgb2	
AC	CE	CV	AC	CE	CV
79	1.1	0.37	73	1.02	0.4
2.66	0.73	0.81	3.9	1.07	1.97
17.39	0.9	1.03	20.41	1.06	1.2
375	0.75	0.53	378	0.75	0.51
1.26	0.82	0.44	1.23	0.8	0.37
0.08	0.55	0.88	0.1	0.74	1
72	1.01	0.44	68	0.95	0.4
38.05	1.1	0.45	44.65	1.3	0.51
145.7	0.4	1.14	470.7	1.29	3.9
48.07	1.1	0.41	51.5	1.18	0.46
262.8	0.89	0.32	277.9	0.94	0.26
16	1.11	0.64	15	1.06	0.68
21.17	0.91	0.52	18.29	0.79	0.41
11.46	0.88	0.53	11.84	0.91	0.51
2.52	1.18	2.18	1.74	0.81	1.59
1694	1.15	0.48	2002	1.36	0.56
1.1	0.8	0.6	1.16	0.85	0.56
21.3	0.76	0.61	21.8	0.78	0.44
48.7	0.7	0.75	77.4	1.12	1.44
987	1.11	0.53	1071	1.21	0.77
8.21	0.76	0.43	7.97	0.74	0.48
1.44	1	1.14	1.7	1.19	1.14
0.96	0.9	0.61	1.19	1.13	0.71
24.41	0.6	0.41	28.45	0.69	0.59
0.23	0.93	1.02	0.24	0.98	1.29
1.82	0.87	0.36	1.84	0.88	0.57
153.6	0.99	0.64	141.3	0.91	0.63
4.21	0.8	0.48	4.01	0.76	0.48
14,292	1.08	0.74	23,726	1.79	1.3
1.51	0.77	0.41	1.52	0.77	0.51
226.7	1.11	0.48	315.1	1.54	0.82
1.33	0.89	0.61	1.32	0.88	0.54
25.77	1.05	0.36	22.65	0.92	0.36
69.3	1.01	0.37	79.19	1.16	0.42
351	1.13	0.81	316.7	1.02	0.97
55.69	0.97	0.22	51.25	0.89	0.28
14.36	1.02	0.29	14.64	1.04	0.3
11.53	1.05	0.42	14.57	1.33	0.6
1.52	1.01	0.88	1.8	1.2	0.66
2.06	1.19	0.78	2.05	1.18	0.7
0.71	0.73	0.83	0.84	0.86	0.67
0.71	0.54	0.57	0.76	0.57	0.8

Remark: Units for oxide is "%"; for Au, Pt, Pd, Ag, Hg, Cd is "ng/g"; & for other is "μg/g".

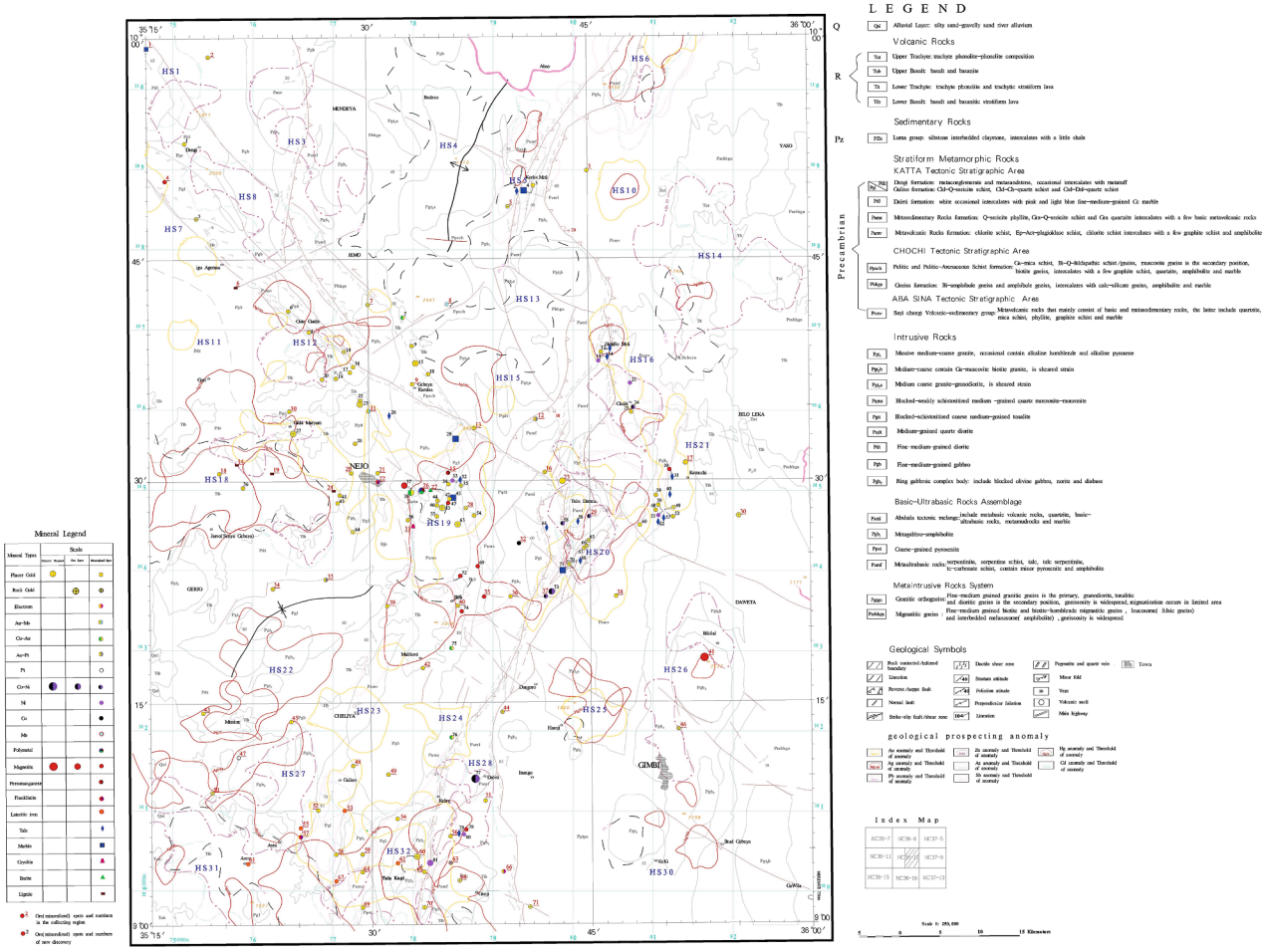

Fig. 4. Composite geochemical anomalies map showing the distribution of Au-Ag-Pb-Zn-As-Sb-Hg-Cd concentration related to geological features of Gimbi-Nejo area with different geochemical anomalous zones (HS).

[Co-Cr], and 7 Fe) (Fig. 4). Further, the following anomalous zones, HS12, HS16, HS18, HS19, HS20, and HS28, could be of valuable mineral exploration.

5. Discussion

5.1. Distribution and variation of ore-forming elements

According to the distribution model test (multi-geo-spatial data management and analysis system GeoExpl 2005 program for calculation, Yao et al., 2011), ore-forming elements in the study area essentially display normal or lognormal distribution. The histograms of each geological formation, which are shown on individual geochemical anomaly maps, suggest that the distribution of Ag, Pb, W, Sn, Be, Mo, La, Li, Sr, Th, U, Ti, F, P, Al_2O_3, Au, Pt, Pd, Ni, Ba, Nb, Rb, Sb, K_2O are symmetrical; but these are negatively skewed for Cu, Zn, Cd, As, Hg, Y, Mn, Co, V, Bi, CaO, Na_2O, SiO_2, and inversely positively skewed for MgO. The distributions of B, Zr are bimodal, and Cr is multi-modal. (Ren et al., 1993). The Chinese background statistical values of stream sediments were obtained from 1:200,000 scale geochemical sampling of 48 map sheets sharing similar geological settings with the studied area (Table 4). Based on these backgrounds, comparison with the average contents of elements in stream sediment samples collected from the study area shows that transitional metals (Au, Cu, Cr, Ni, Co, V, Ti, Mn, Fe_2O_3, Zr, Nb), non-metal (P), alkaline earth elements (Ba, Sr), and basic metal (Al_2O_3) in the study area are higher, while the contents of As, Sb, Bi, Hg, B, Be, W, Sn, La, Li, Th, Cd, Pb, F, Na_2O, and K_2O are lower. However, the most significant difference is represented by the values of Hg, Sb, and As contents in the area, which are two to three times lower than the recommended respective contents (Table 4). The low content of Hg, Sb, As, and high iron group elements distribution may be attributed to the extensive occurrence of basic-ultrabasic rocks within the Precambrian metamorphic terrane of the region.

The variation of elements concentration was measured by determining the coefficient of variation; $CV\ (\%) = S/X*100$, where CV is coefficient of variation, S indicates standard deviation, and X is mean concentration. The coefficient of variation was utilized to evaluate the degree of elemental differentiation in the Gimbi-Nejo area (Table 2). The main types of element differentiation related to the major geological processes that were active in the area, including enrichment of Au, As, B, Bi by *meta*-volcanic and sedimentation; syngenetic enrichment of Cu, Pt, Pd, Cr, Ni, V, Ti, etc. by basic-ultrabasic magmatic events; dilution of Hg, Bi, As, Sb, etc. concentrations by metamorphism; and enrichment of Au, As, Sb, Hg, etc. as the result of hydrothermal activities. The enrichment of the main ore-forming elements and their associated components in the study area are related to locations of intense differentiation, which

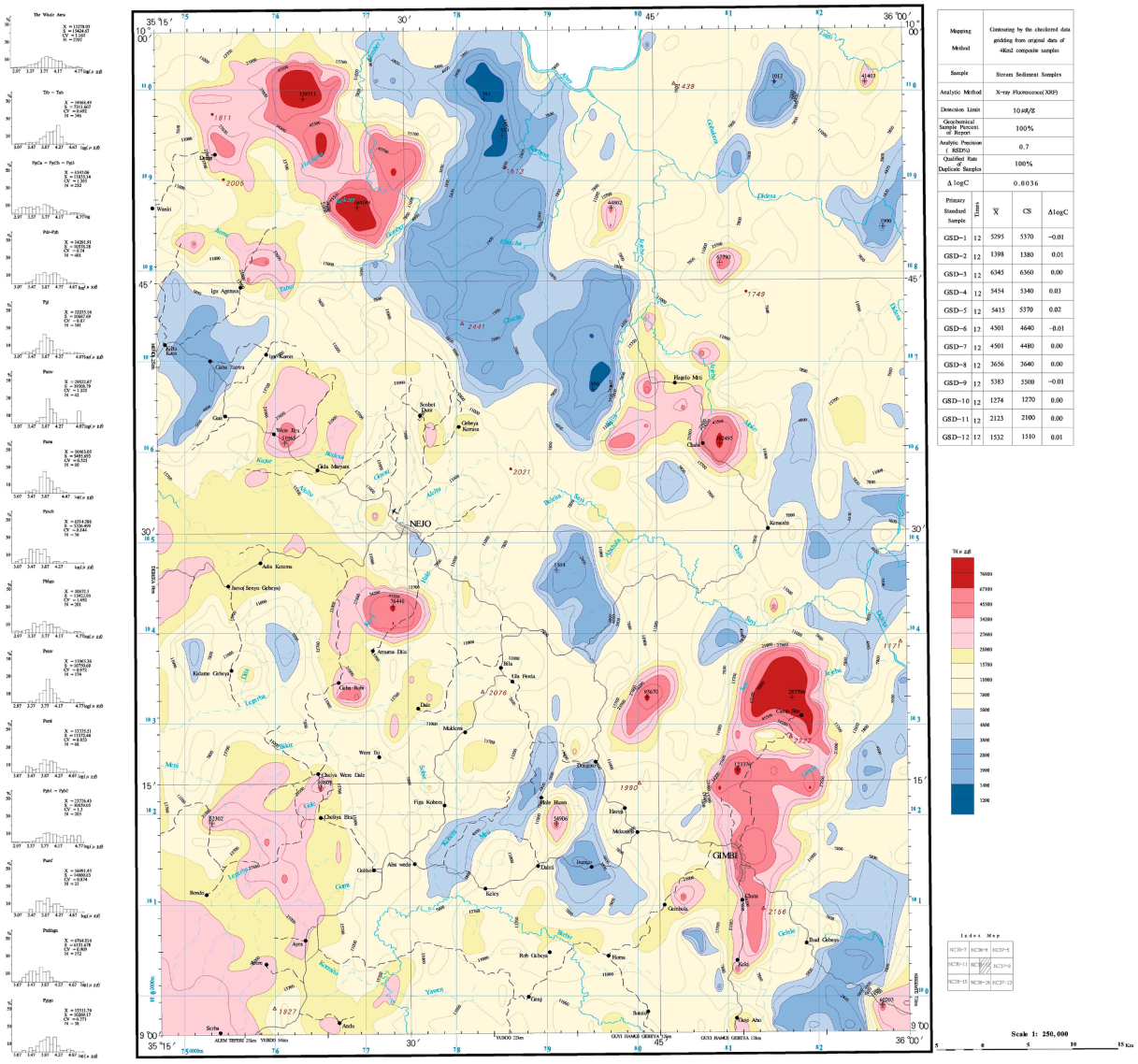

Mapping Method	Contouring by the checkered data gridding from original data of 4Km2 composite samples		
Sample	Stream Sediment Samples		
Analytic Method	X-ray Fluorescence(XRF)		
Detection Limit	10 μg/g		
Geochemical Sample Percent of Report	100%		
Analytic Precision (RSD%)	0.7		
Qualified Rate of Duplicate Samples	100%		
Δ logC	0.0036		
Primary Standard Sample	Times	$\bar{X}$	CS	ΔlogC
GSD-1	12	5295	5370	−0.01
GSD-2	12	1398	1380	0.01
GSD-3	12	6345	6360	0.00
GSD-4	12	5454	5340	0.03
GSD-5	12	5415	5370	0.02
GSD-6	12	4501	4640	−0.01
GSD-7	12	4501	4480	0.00
GSD-8	12	3656	3640	0.00
GSD-9	12	5383	5500	−0.01
GSD-10	12	1274	1270	0.00
GSD-11	12	2123	2100	0.00
GSD-12	12	1532	1510	0.01

Fig. 5. Geochemical map showing the distribution of "Ti" concentration in the Gimbi-Nejo area, West Ethiopia.

are thus the focus of exploration.

5.2. *Ore-forming element enrichments in geological formations*

Ore-forming elements are enriched in the Precambrian to Tertiary exposed rocks in the study area. The average contents, coefficient of variation, and enrichment factor of all considered elements in each stratigraphic unit are shown in Table 5. This regional geochemical information introduces new geochemical backgrounds for Ethiopia's most common geological domains. The analysis of each geological formation hosting chalcophile, siderophile, and lithophile elements are shown in five composite geochemical maps and are briefly descripted below.

5.2.1. *Metamorphosed intrusive rock units*

Migmatitic gneiss (Pmbhgn) and Granitic orthogneiss (Pgtgn) are two Precambrian metamorphosed intrusive rocks in the study area (Fig. 2). In the Pmbhgn, strong differentiation of Au As, B, Cr, Ni (≥1.0) indicates that partial enrichments are due to later superimposed hydrothermal activities and intermediate to basic components of the intrusion. In the Pgtgn, strong differentiation of the high background elements (Pd, Ag, Th, U, La, F, Y, Be, P, Ti, Hg, SiO_2) also suggests the superposition of late hydrothermal activities as the essential cause of the local geochemical anomalies (Fig. 4).

5.2.2. *Precambrian aba sina domain*

In this domain, Sayi Chenga volcanic-sedimentary formation (Psmv) is distributed on the north–south trending zone on the east side of the Belete shear zone. The Psmv is characterized by enrichment of MgO, Na_2O, and CaO with high average contents of Au, Zn, As, Sb, B, Cd, Cu, Pt, Pd, Cr, Ni, Co, W, Sn, and low contents of Zr, Y, Nb, Rb, U, La, Th. The strong differentiation of Au, As, Sb, and B suggests the superposition of syn. to late hydrothermal activities. The composite anomalies of Au, Zn, As, and Sb appear here as the indicator of mineralization (Fig. 4).

5.2.3. *Precambrian Chochi domain*

The Precambrian Chochi domain consists of gneiss (Pbhgn) and pelitic-arenaceous schists (Ppsch). Pbhgn is located in the central north side of the work area with poor abundances of Au, As, Sb, Hg, associated with siderophile elements, rare earth and radioactive elements, high background - enrichment of CaO, Na_2O, K_2O, SiO_2, MgO, Ba, Rb, Sr, Bi

Table 6
A geochemical anomalous zone HS16 contains dominant elements characteristic values.

Element	Au	Pt	Pd	Cu	Ag	Zn	As	Sb	Ni	Co	Cr
Area (km^2)	40	76	48	92	32	52	36	32	80	24	96
Shape	zonal	oval	oval	zonal	oval	oval	oval	irregular	zonal	oval	oval
Maximum value	13.6	8.2	6.9	145.9	212.0	228.1	23.1	1.64	716.9	103.5	12,912
Average value	6.44	2.66	4.2	89.1	144.0	138.9	15.8	0.82	252.3	80.1	2522
Contrast	1.84	1.77	1.68	1.27	1.44	1.46	1.76	2.05	2.52	1.34	5.05
Dimensions	73.6	134.5	80.6	116.8	46.1	75.9	63.4	65.6	201.6	32.16	484.8

Remark: Units for Au, Pt, Pd, Ag is "ng/g"; & for other is "μg/g".

and weak enrichment of W. The coefficient of variation of Bi (3.12 %) and W (1.69 %) in Pbhgn is indicative of strongly non-uniformal distribution. There are superpositions of medium–high temperature hydrothermal activities as a cause of partial W & Bi anomalies. The strong differentiation of Au, As, B, Cr, and Ni suggests the superposition of local hydrothermal activities and the late intrusion with intermediate-basic components. Ppsch has distributed within Chochi and Digiro river with poor contents of Au, Hg, Cr, Ni, Ti, Pt, Pd and enriched contents of Ba, Th, Rb, Sr, Li, U, W, Pb, B, Na_2O, and K_2O. In the Chochi domain, all anomalies suggest the superposition of magmatic-hydrothermal mineralization-related activities (Fig. 4).

5.2.4. Precambrian Kata domain

The Precambrian Kata domain contains *meta*-volcanic (Pamv) and *meta*-sedimentary formation (Pams) of the

Aleltu group and Guliso formation (Pgl) of the Bila group. Pamv is distributed in the Chochi shear zone in the northwest of the working area. The statistical results of samples show the high contents of W, Zn, Mn, V, Ti, Fe_2O_3 and the most deficient contents of Pb, La, Nb, Be, Rb, K_2O in the whole domain (Tadesse et al., 2003). According to the degree of elemental differentiation, the coefficient of variation of Ag, Cu, and Zn is <0.5 μg/g, showing uniform distribution. The strong differentiation of Au, As, Pt, Pd, W, and Bi reflects the superposition of hydrothermal activities. The Pams is located west of the Belete shear zone and south of the Chochi shear zone. Strong differentiation of W, Bi, Ba, and Cr in this formation also suggests hydrothermal activities. The partial anomalies of W, Sn, Bi, and Mo reflect the effect of late superposition by the acidic component intrusion. The Pgl is one of the most critical formations for Au enrichment. Its elements differentiations of Cr, Ni, Pt, and Pd also reflect the late superimposed intrusion of intermediate-basic components in Pgl (Fig. 4).

5.2.5. Meta-basic to ultra-basic rocks

This rock unit was composed of Abshala tectonic melange (Paml) and meta-ultrabasic rocks (Pumf). The Paml is distributed in Belete NS-trending shear zone with strong differentiation of Au, As, B, Sb, Cr, Ni, Co, Pt, and Pd reflecting superimposed enrichment of the late hydrothermal mineralization events. Au displays an enrichment trend with the metabasic - ultrabasic component in the same period. The Pumf is also distributed in the Belete NS-trending shear zone with strong Au, As, and Sb differentiation, reflecting superimposed hydrothermal mineralization events. Au has the ore-forming tendency to accompany Pt, Cu, Cr & Ni in rock units. The differentiation of Sn with low content reflects the superposition of the late hydrothermal activity (Fig. 4).

5.2.6. Metagabbro-amphibolite and gabbroic complex (Pgb1/Pgb2)

The basic intrusive rocks in the work area were previously divided into metagabbro-amphibolite (Pgb1) and annular gabbroic complex rock (Pgb2). These are mainly-three parallel zonal distributions with the north–south direction of the Tulu Dimtu structural zone. The strong differentiation of Cr and Ni indicates enrichment of late superimposed hydrothermal events. The Au coefficient of variation reaches up to 1.6 %, showing strongly non-uniformal distribution, associated with strong differentiation elements (As, Sb & B), suggesting the superimposed mineralization of the late low-temperature hydrothermal activity (Fig. 4).

5.2.7. Intermediate-basic (Pdt &Pgb) and acidic intrusive rocks (Pgt3 & Pgt2)

The intermediate-basic intrusive rocks are distributed in the Dengi litho-tectonic domain to the west of Belete NS trend shear zone and south of Chochi NW trend shear zone, covering an exposed area of 1604 km^2. Statistical data show that Au, Cr, Pd, B, Ti, and Sb have strong differentiation. The Au coefficient of variation reaches up to 2.18 ng/g. Its distribution is uneven, indicating mineralization by the late tectonic hydrothermal activity in the Chochi shear zone. It leads to Au enrichment by hydrothermal migration within intermediate-mafic intrusive rocks in the vicinity of the shear zones and southwest side of Chochi shear zone.

The Pgt3 & Pgt2 rocks are widely spread in the work area of 928 km^2. The enriched elements W, Sn, Be, Bi, Ba, Rb, Th, U, SiO_2, Na_2O, and K_2O were essentially of granite characteristics. The strong differentiation of Au, As, Hg, B, W, Bi, Mo, Th, Nb, Cr, Ni, Co, V, and Ti indicate superimposed enrichment related to magmatic-hydrothermal mineralization activities, which leads to the Zr, La, Nb, Rb, Yu, Th series, and W, Sn, Bi, Mo series covering a large area of granite. In the acidic rocks, local fractionation and concentration of Cr, Ni, Co, V, Ti, and siderophile elements may also suggest the presence of superimposed basic-ultrabasic intrusion (Fig. 4).

5.2.8. Tertiary volcanic rocks

These rocks with multi-element enrichment are distributed in the southwest and northeast of the work area (1384 km^2). In this lithologic unit, strong differentiation of Au and B indicates the superimposition of partial weak mineralization (Fig. 4); apart from that, other high background elements (Ag, Zn, Pb, Hg, and Cd) are uniformly distributed. In such case of no significant differentiation, mineralization is limited to *syn*-magmatism, and the late superimposed hydrothermal mineralization is not significant.

5.3. Characteristic of geochemical anomalous zones

The studied areas in Gimbi-Nejo can be further divided into thirty-two distinct anomalous zones (HS) based on dimension, intensity, geological environment, and spatial association of the ore-forming elements. Each zone is characterized by several dominant ore-forming elements (Table 3). The statistical values suggest that distribution of these elements are associated principally with the following geological features: tectonic hydrothermal activities (I), meta-basic and meta-ultrabasic rocks (II), metamorphosed volcanic and sedimentary rocks (III), intermediate-acid intrusive rocks (IV), intermediate-mafic intrusive rocks (V), and Tertiary volcanic lava (VI) (Table 3). In the study area, most important anomalous zones are HS5, HS12, HS16, HS19, HS21, and HS28 for the vital inspection, while HS11, HS18 HS20, HS25, and HS32 are for reconnaissance inspection. The primary anomalous zone typically contains strong serpentinization, talcization, and

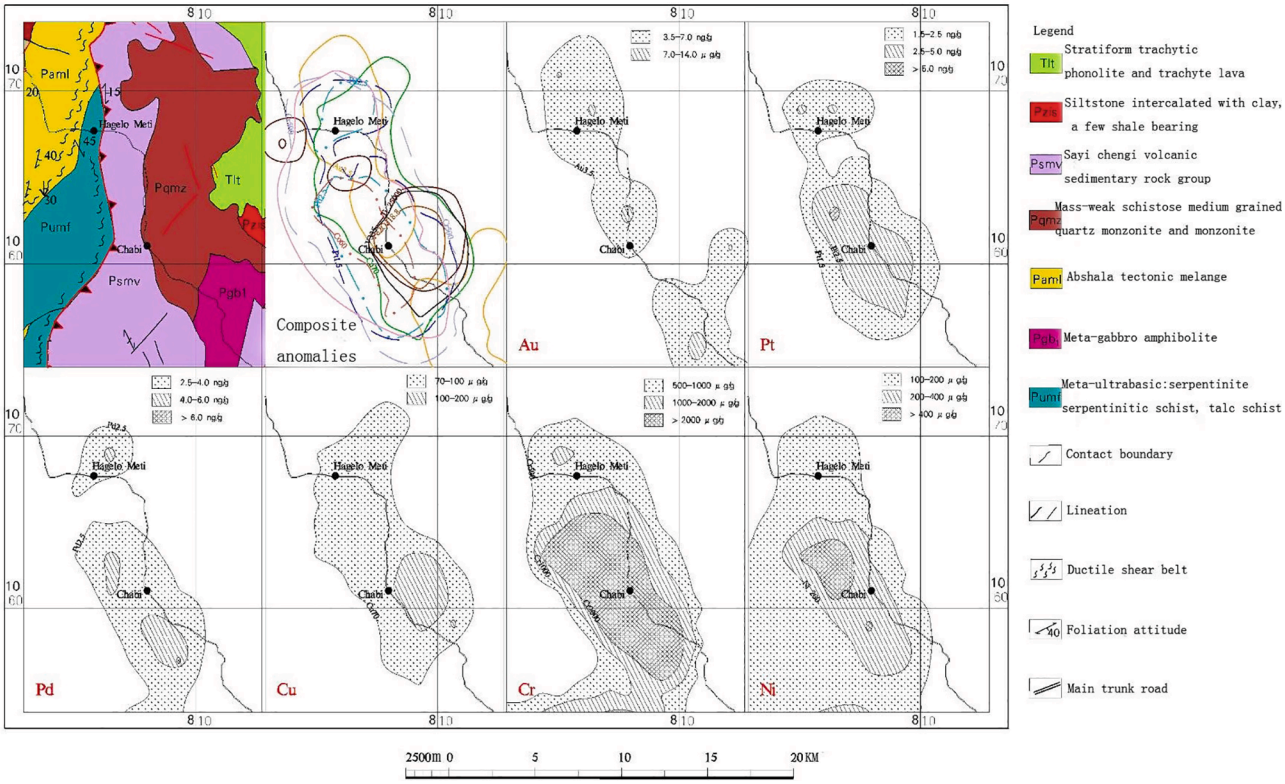

Fig. 6. Geochemical anomalous zone map of HS16 showing composite anomalies of Au, Cu, Pt, Pd, Cr, and Ni.

silicification in meta-ultrabasic rocks with nickel, platinum, and chromium enrichments. Some anomalous zones have sulfide-bearing quartz veins controlled by a northwest-trending shear zone with high gold and copper mineral potentials. In the HS20 anomalous zone, nickel, gold, and cobalt mineralization were found in Tulu Dimtu.

Most importantly, the geochemical anomalous zone HS16 contains Au, Pt, Pd, Cu, Cr, and Ni composite anomalies (Table 6, Fig. 4). This likely specific zone is located in the Hagelo meti area at the center-northern section of the Belete shear zone, between latitudes 9°32′~9°42′N and longitudes 35°45′~35°51′E. It consists of Abshala tectonic mélange, meta-ultrabasic rocks, meta-gabbro amphibolite, Sayi chenga volcanic-sedimentary rocks, siltstone interbedded with claystone and shale (Luma), schistositized medium-grained quartz monzonite-monzonite, and trachyte lava (Fig. 6). These rocks well developed serpentinization, steatitization, chloritization, contain quartz veinlets in the fissures, and are weakly mineralized. In fact, several types of ore sites can be determined in the HS16, including two placer gold ore spots, one nickel (cobalt) mineralized spot, two mineralized nickel spots, and two talc mineralized spots. In considering the mineralization associations in the zone (HS16), two composite anomalous series, Cu-Pt-Pd-Cr-Ni-Co-V and Au-Ag-As-Sb-Cd, can be distinguished in the northwest direction about 15 km in length and 12 km in width. Au, Pt, Pd, and Cu anomalies are closely coexisting in zone, and the peak values are up to13.6 ng/g, 8.2 ng/g, 6.9 ng/g, and 145.9 μg/g, respectively. The oval-contoured Ag, As, and Sb anomalies partly overlapped within the north and south ends of the zone, while Cr, Ni, and Co anomalies are completely overlapped. The results of the 1:50,000 scale stream sediment survey show that Au, Cu, Pt, and Pd anomalies have good reproducibility, and the intensity is significantly increased in HS16. These anomalies are contoured 5 km^2 northern and 11 km^2 southern by the threshold limit respectively 5.0 ng/g, 100 μg/g, 3.5 ng/g, and 8.0 ng/g (Fig. 7). The maximum contents of Au, Cu, Pt, Pd, Cr, and Ni in this zone are 15.0 ng/g, 186.1 μg/g, 11.4 ng/g, 24.7 ng/g, 79739.2 μg/g, and 1819.0 μg/g (Table 6). According to the data from the 1:10,000 scale soil profile, it can be seen that there is intense Pt, Pd, Cr, and Ni mineralization showing in altered rocks (Pumf), the peak values of Pt, Pd, Cr, and Ni, respectively are 10.8 ng/g, 20.7 ng/g, 13627 μg/g, and 2473 μg/g (Fig. 8). The obtained geochemical mapping data of the whole study area suggest that the anomalous zones, HS12, HS16, HS18, HS19, HS20, and HS28, could be the favorable focus of exploration. Based on our geochemical mapping results, one Chinese mineral company (Mindi mining PLC) has started working in an anomalous zone (HS28) to explore Ni and Co.

5.4. Excavation testing

In order to ensure the accurate information of ore-forming elements in stream sediments, multiple exploration methods, including geological traverse section, exploratory trenches, shallow shaft, drill hole testing, etc., were adopted, and >60 mineral deposits have been found. The mineral separation has been conducted in the high anomalous zones like HS12, HS16, HS18, HS19, HS20, and HS28. The anomalous zone HS19 is predominant in the study area due to the enrichment of Au, Cu, Pt, and Pd (Fig. 4). In HS19, panning activity is a typical scene in all scales of streams for mineral separation. The placer gold has two sources in HS19, either directly collected from the river channel, or collected by digging the lower part of the gravel stratum near the river channel (Fig. 11c,d). In the Kata area along the HS19, there exists an adit at 0779733N/1049411E, approximately 150 m long. An Au-Cu-bearing quartz vein is on the wall at the entrance with solid carbonation, silicification, chloritization, and epidotization (Fig. 12). The highest Au (S-044-01) value up to 949 ng/g is obtained at the adit entrance (Fig. 10). Due to strong weathering, a sampling section has been excavated 30 m away from the adit entrance. The analytical results are shown in Table 7. In Giba Buraso area along the same HS19, auriferous quartz veins (length 2 km, width 3–15 m) intercalate felsic schist, and sericite-quartz schist has also developed in the N—S direction, with regional schistosity (Fig. 11a, b). The excavation has been done at 0783636E/1047828N to expose the

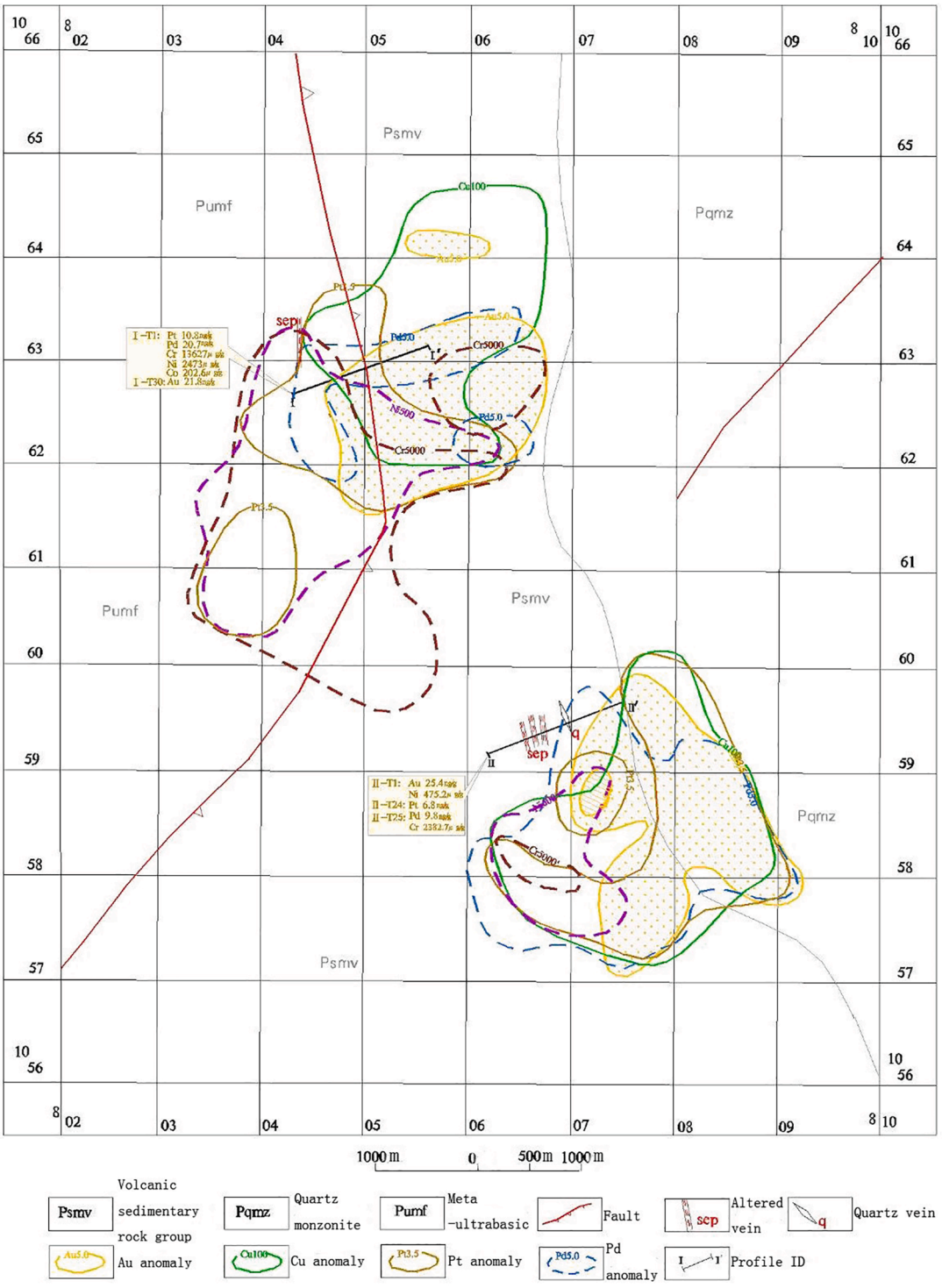

Fig. 7. Geochemical anomalous zone map of HS16 showing geochemical prospecting significance.

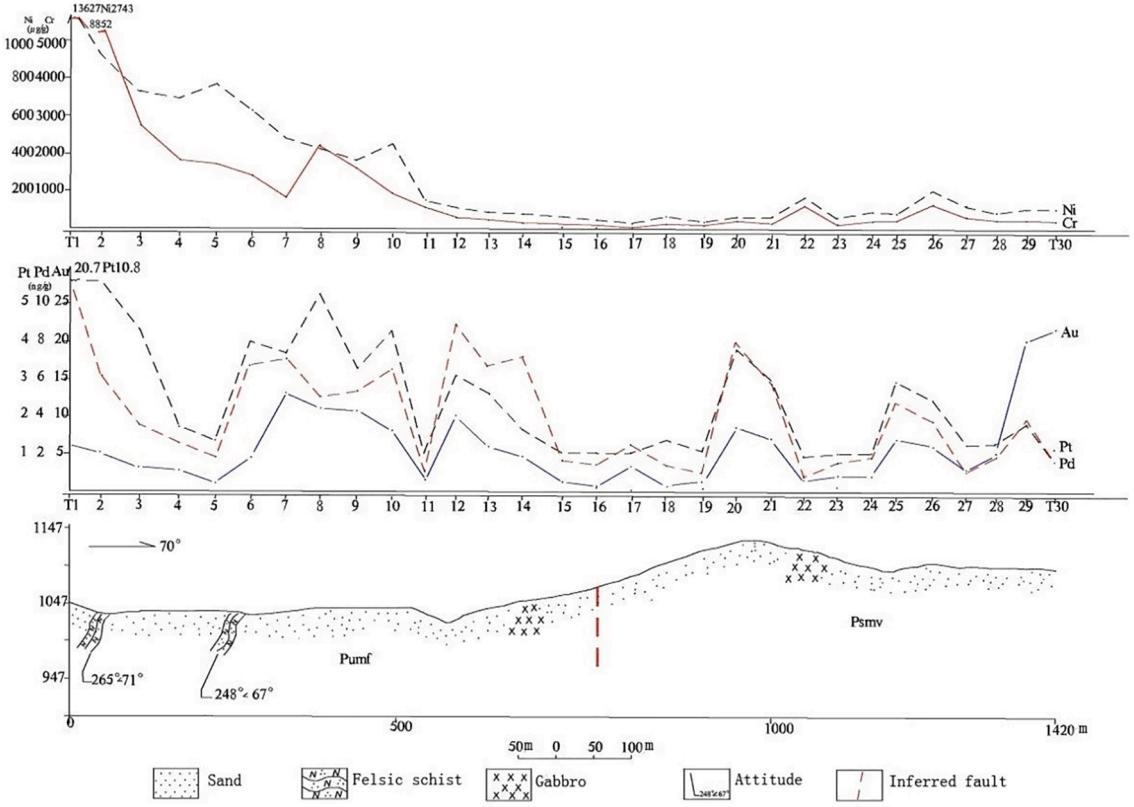

Fig. 8. Soil profile of composite anomalies of the geochemical anomalous zone (HS16).

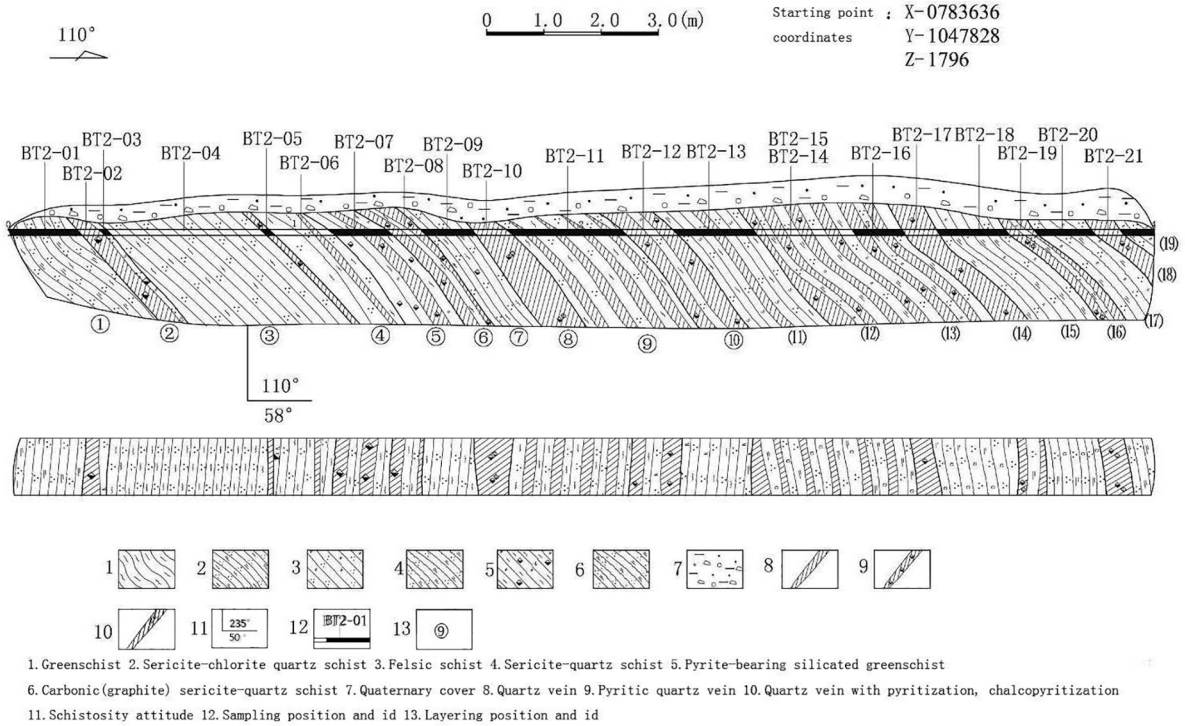

Fig. 9. Sampling profile of BT2 excavation of geochemical anomalous zone (HS19).

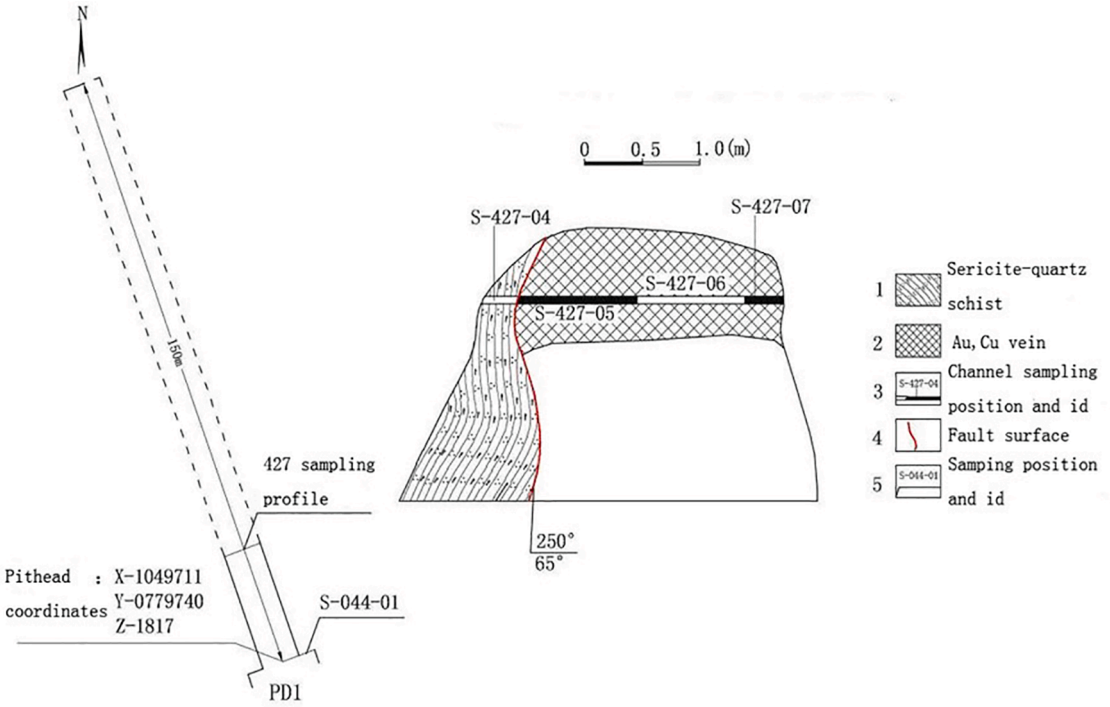

Fig. 10. Sampling profile of adit PD1 of the geochemical anomalous zone (HS19).

Fig. 11. (A) Auriferous quartz vein zone, (B) Outcrop of weathered quartz veins extended in SE direction of BT2, (C) Panning pit on the flooded land of Kata river, (D) Panning activity for placer gold along stream channels.

Fig. 12. Adit for exploration minerals, (A) Gold-bearing quartz vein, (B) Visible gold in quartz vein, (C) Ore deposit contains pyrite and chalcopyrite.

vein system for sampling (Fig. 9). The results present in Table 7 yield the highest Au value of 1.43 ng/g. A traverse survey has also been conducted along the strike of auriferous quartz veins (BT2) to pursue their strike extension. Two grab samples (S-415-02 and S-415-04) were also gathered from weathered quartz veins, located southeast of BT2 (0783522E/1048334N; 0783441E/1049549N), getting Au values of 0.45 ng/g, 0.14 ng/g, respectively, indicating that auriferous quartz veins extend along the strike and show better gold mineralization (Fig. 11a,b). The primary mineralization in the quartz veins was pyrite and chalcopyrite (Fig. 12c). During the microscopice study of core samples, it can be seen that natural gold is filled in the pyrite micropores or mineral gaps (Fig. 13), and gold is mostly irregular shaped or granular. The gold particles are about 1 μm ~ 300 μm, with an average of 11 μm and bright gold is partially visible in the core samples. Same as in other high-intensity values anomalous zone, excavation was done to know the surface extension of ore bodies and drilling at well-mineralized segments.

5.5. Spatial distribution

Geochemical anomaly maps are the main results of the geochemical prospecting. The major ore-forming elements in the research region include Au, Cu, Cr, Ni, Co, V, Ti, Mn, Fe_2O_3, P, Ba, Zr, Sr, Nb, Al_2O_3, and the associated elements are Pb, Cd, La, Li, Sn, U, Th, Rb, Pt, Pd, K_2O, Na_2O, CaO, MgO, Mo, Hg, W, Bi, Sb, As, B, SiO_2, Y, F, Be, Ag, and Zn. Analytical data generate geochemical maps of each ore-forming element to show the possible anomalies and figure out the dispersion haloes. In the geochemical maps, anomalies were delineated based on 85 %, 95 %, and 98.5 % of the cumulative frequency distribution and designated as outer, middle, and inner anomalous zones. The uniform anomaly threshold in the region was the content corresponding to the 85 % value of the cumulative frequency. These geochemical maps suggest that in the study area, mostly transition metals with high whole area average content as compared to Chinese recommended stream sediments values have high economic potentials and are mainly distributed in migmatitic gneiss (Cu ~ 66.38 μg/g), granitic orthogneiss (Zr ~ 426.9 μg/g), upper basalt/lower basalt(Nb ~ 63.4 μg/g) rocks, meta-basic (Mn ~ 2680 μg/g, Ti ~ 29823 μg/g, V ~ 365.6 μg/g, Fe_2O_3 ~ 16290000 μg/g) rocks, meta-sedimentary formation (Au ~ 0.0053 μg/g), Abshala tectonic melange (Cr ~ 2457.1 μg/g), and meta-ultrabasic rocks (Co ~ 62.65 μg/g, Cu ~ 66.38 μg/g, Ni ~ 313.4 μg/g). The composite maps of ore-forming elements were also generated to represent the absolute concentration of ore forming elements in each rock unit with anomalous geochemical zone (HS) elements (Table 3) associated with geological features (Fig. 4). The obtained data of geochemical prospecting indicates 64 new mineralized spots in the study area, including 31 Au, 16 Cu, 10 Ni (Co-Cr), and 7 Fe. During geological field work also marked some new non-metallic minerals spots including talc, marble, cryolite, barite, lignite, etc. All these mineralized spots are present in composite maps (Fig. 4). Further studies are strongly recommended to raise the degree of essential geological and mineral resource exploration in west Ethiopia.

6. Conclusions

1. The present geochemical prospecting was conducted for forty-two ore-forming elements in a 9100 km^2 area of the Gimbi-Nejo in west Ethiopia. After strict data monitoring, geochemical anomaly maps of stream sediments were generated, which shows the possible anomalies of interested elements and explain their dispersion haloes. The composite maps of ore-forming elements were also established

Table 7
A geochemical assay results of samples taken from excavation.

Sample No.	Rock (Ore) Name	Au	Ag	Cu	Zn	Pb	As
BT2-01	Chlorite-quartz schist	0.013	0.057	55.49	120.2	8.665	95.02
BT2-02	Quartz veins bearing Pyrite	<0.005	0.035	32.28	57.22	2.306	3.71
BT2-03	Silicified-pyritized schist	<0.005	0.088	20.6	6.692	6.428	7.59
BT2-04	Chlorite-quartz schist	0.009	0.244	31.38	98.79	15.08	168.83
BT2-05	Quartz veins bearing Pyrite	0.013	0.235	25.95	24.16	8.761	28.99
BT2-06	Chlorite-quartz schist bearing a few of fine quartz veins (0.5 cm)	0.01	0.645	57.46	116.7	41.48	94.93
BT2-07	Interbed of fine Py-quartz veins and sericite-chlorite-quartz schist	0.007	0.197	135.4	51.63	10.06	57.22
BT2-08	Py quartz vein bearing green schist lens (10 cm)	<0.005	0.133	86.74	104.9	4.431	22.48
BT2-09	Sericite-chlorite-quartz schist bearing a bit fine-grained Py	0.006	0.196	69.78	106.9	5.771	56.23
BT2-10	Py-Cpy quartz veins	<0.005	0.1	188.8	14.35	5.817	33.43
BT2-11	Chlorite-quartz schist bearing fine quartz veins	<0.005	0.163	45.44	82.67	7.288	69.55
BT2-12	Py quartz veins intercalated with chlorite felsic schist	<0.005	0.091	34.67	41.85	6.421	15.06
BT2-13	Chlorite-felsic schist bearing quartz veinlet	1.43	0.145	28.29	123.2	43.88	76.36
BT2-14	Quartz veins	<0.005	0.091	67.58	17.99	8.583	14
BT2-15	Sericite schist	0.014	0.196	83.55	81.33	7.943	52.43
BT2-16	Sericite schist	0.024	0.272	100.8	51.27	9.001	87.37
BT2-17	Py quartz vein	<0.005	0.105	112.3	54.22	3.565	22.12
BT2-18	Sericite-quartz schist	0.026	0.44	229.1	88.42	16.87	108.9
BT2-19	Py-Cpy quartz veinlet overlapped with carbonaceous sericite-quartz schist	0.015	0.189	153.3	49.63	5.357	37.42
BT2-20	Sericite-quartz schist	0.018	0.349	190.9	84	10.35	47.43
BT2-21	Sericite-quartz schist	<0.005	0.043	19.59	7.556	7.119	5.37
S-415-01	Quartz veins	0.092	0.056	–	–	–	–
S-415-02	Quartz veins	0.451	0.055	–	–	–	–
S-415-03	Quartz veins	0.011	0.061	–	–	–	–
S-415-04	Quartz veins	0.14	0.22	–	–	–	–
S-427-04	Silicified sericite-quartz schist	0.00153	0.971	1623	251.7	37.21	11.48
S-427-05	Limonitized ore rocks	0.333	0.14	469.6	53.9	6.703	17.75
S-427-06	Limonitized ore rocks	0.001672	0.15	348.8	46.43	3.36	1.75
S-427-06B	Limonitized ore rocks	0.000452	0.05	78.38	10.56	3.122	1.43
S-427-07	Limonitized ore rocks	1.11	0.131	1531	753.1	4.09	15.98
S-044-01	Silicified sericite-quartz schist	0.949	–	1380	40.4	24.5	–
S-427-02	Ore rocks bearing Py, Cpy, calcite-quartz dikes	0.0648	0.258	1193	19.6	10.27	42.11
S-427-03	Ore rocks bearing Py, Cpy, calcite-quartz dikes	2.02	1.247	24,660	125.9	13.38	30.38

Remark: Unit is "μg/g"; Py: pyrite, Cpy: chalcopyrite.

Fig. 13. (A) Core sample bearing quartz vein, (B) Drilling samples of ore deposits, (C) & (D) Microscopic image showing pyrite mineral containing gold in the cavity.

to represent the absolute concentration of ore-forming elements in each lithologic unit.

2. The ore-forming element-enriched areas are divided into thirty-two distinct composite anomalous zones (HS). Among them, HS12, HS16, HS18, HS19, HS20, and HS28 could be the favorable focus of exploration due to intense differentiation.
3. In the study area, SiO_2, Al_2O_3, Y, F, Be, Ag, and Zn with coefficient of variation < 0.5 were identified as uniform distribution; elements with coefficient of variation $0.5 \sim 0.7$, such as Cu, Pb, Cd, La, Li, Sn, Fe_2O_3, Mn, Co, P, and U, display relatively uniform distribution pattern; Zr, Th, Rb, Nb, Sr, Ba, Pt, Pd, K_2O, Na_2O, CaO, MgO, V, Mo, and Hg with coefficient of variation $0.7 \sim 1.0$ were considered as differentiation; Ni, Cr, Ti, W, Bi, Au, Sb, As, and B elements with coefficient of variation ≥ 1.0 were identified as strong differentiation within the ore-forming minerals. The obtained geochemical mapping indicates strong anomalies and thus high economic potentials for Au (2.14 ng/g), Cu (43.56 μg/g), Cr (365.1 μg/g), Ni (69.2 μg/g), Co (34.46 μg/g), V (204.1 μg/g), Ti (13278 μg/g), Mn (1472 μg/g), Fe_2O_3 (10.97 %), P (888 μg/g), Al_2O_3 (14.05 %), Ba (501.7 μg/g), Zr (309.5 μg/g), Sr (155.7 μg/g), and Nb (28.2 μg/g).
4. According to the regional geological setting of the area, composite geochemical maps suggest that the intermediate-acidic and basic intrusive rocks, meta-sedimentary rocks, meta-basic, and meta-ultrabasic rocks, tertiary volcanic lava, and tectonic hydrothermal activities along the north–south structural belt have the dominant controlling role for regional mineralization.

Declaration of Competing Interest

The authors declare that they have no known competing financial interests or personal relationships that could have appeared to influence the work reported in this paper.

Data availability

Data will be made available on request.

Acknowledgments

This study was made possible by the cooperation of the Chinese Ministry of Commerce, China Science and Technology Ministry, the Chinese Ministry of Natural Resources, and the Ethiopian Ministry of Mines and Energy. We thank all project members from Wuhan Center, China Geological Survey, Geophysical Exploration Brigade of Hubei Geological Bureau, and Geological Survey of Ethiopia, who collected and combined samples for the project. Special thanks to the People's Republic of China Embassy in Ethiopia for their support during works. We also acknowledge the following laboratories' analytical support: Testing Center of Wuhan Institute of Geology and Minerals Resources, and ALS Chemex (Guangzhou) Co. Ltd. We also thanked Dr. Zhang Weifeng for preliminary review, Prof. Wang Rucheng and Isaak Swan for proof reading, Editor-in-chief Huayong Chen, and the anonymous reviewers for critical comments and constructive suggestions, which improved the quality of the paper.

Funding

This work was supported by the Economical Supporting Fund of China Commerce Ministry (Foreign-aid project (2007)420) and China Science and Technology Ministry (International cooperation project no. 2009DFA20630).

Appendix A. Supplementary data

Supplementary data to this article can be found online at https://doi.org/10.1016/j.oregeorev.2022.105117.

References

Abera, S., 1994. Review of industrial minerals of ethiopia. AGID Rep. Ser. Geosci. Int. Dev. 18, 173–180.
Appleton, J.D., Ridgway, J., 1992. Regional geochemical mapping in developing countries and is application to environmental studies. Appl. Geochem. 2, 103–110.
Arndt, N.T., Fontboté, L., Hedenquist, J.W., Kesler, S.E., Thompson, J.F.H., Wood, D.G., 2017. Section 2Formation of mineral deposits. Geochem. Perspect. 6 (1), 18–51.
Asrat, A., Barbey, P., Gleizes, G., 2001. The precambrian geology of ethiopia: a review. Afr. Geosci. Rev. 8 (3/4), 271–288.
Getaneh, A., 1985. The mineral industry of Ethiopia: present conditions and future prospects. J. Afr. Earth Sci. 3 (3), 331–345.
Ayalew, T., Peccerillo, A., 1998. Petrology and geochemistry of the Gore-Gambella pultonic rocks:implications for magma genesis and the tectonic setting of the Pan-Aftrican orogenic belt of western Ethiopia. J. Afr. Earth Sci. 27 (3/4), 397–416.
Beckhoff, B., Kanngießer, B., Langhoff, N., Wedell, R., Wolff, H., 2006. Handbook of Practical X-Ray Fluorescence Analysis, Springer, ISBN 3-540-28603-9.
Belete, K.H., Mogessie, A., Hoinkes, G., Hettinger, K., 2000. Platinum-group minerals and chrome-spinels in the Yubdo ultramafic rocks, western Ethiopia. J. Afr. Earth Sci. 30, 10–11.
Billay, A.Y., Kisters, A.F.M., Meyer, F.M., Schneider, J., 1997. The geology of the Lega Dembi gold deposit southern Ethiopia: implications for Pan-African gold exploration [J]. Miner. Deposita 32 (5), 491–504.
Briggs, P.H., 2002, The determination of forty elements in geological and botanical samples by inductively coupled plasma-atomic emission spectrometry, chap. G of Taggart, J.E., Jr., ed., Analytical methods for chemical analysis of geologic and other materials, U.S. Geological Survey: U.S. Geological Survey Open-File Report 02-223, 18 p.
Chandrajith, R., Dissanayake, C.B., Tobschall, H.J., 2001. Enrichment of high field strength elements in stream sediments of a granulite terrain in Sri Lanka – evidence for a mineralized belt. Chem. Geo. 175 (3-4), 259–271.
Cheng, Z., Xie, X., Yao, W., Feng, J., Zhang, Q., Fang, J., 2014. Multi-element geochemical mapping in Southern China. J. Geochem. Explor. 139, 183–192. https://doi.org/10.1016/j.gexplo.2013.06.003.
Cooley, Elmo F., Curry, Kenneth J., Carlson, Robert R., 1976. Analysis for the Platinum Group Metals and Gold by Fire-Assay Emission Spectrography. as/30/1/as-30-1-52.pdf, 30(1), 52–56. doi:10.1366/000370276774456598.
Darnley, A.G., 1990. International geochemical mapping: a new global project. J. Geochem. Explor. 39 (1-2), 1–13.
Deksissa, D.J., Koeberl, C., 2002. Geochemistry and petrography of gold-quartz-tourmaline veins of the Okote area, southern Ethiopia: implications for gold exploration [J]. Mineral Petrol. 75 (1), 101–122.
Deksissa, D.J., Koeberl, C., 2004. Geochemistry, alteration, and genesis of gold mineralization in the Okote area, southern Ethiopia [J]. Geochem. J. 38 (4), 307–331.
Fentaw, H.M., Mohammed, S., 1999. Geology and economic aspect of the Moyale graphite deposit. Ethio-Norwegian Report, 99-002, EIGS, Addis Ababa, 53 p.
Fentaw, H.M., Mengistu, T., 1998. Comparison of Bombowha and Kombelcha kaolins of Ethiopia. J. Appl. Clay Sci. 13, 149–164.
Ficklin, W. K., 1970 A Rapid Method for the Determination of Fluoride in Rocks and Soils, Using an Ion-Selective Electrode United States Geological Survey, Professional Paper 700: pp. 186–1 88.
Fletcher W.K., 1997. Stream sediment geochemistry in today's exploration world. In: A. G. Gubbins (ed.), Proceeding of exploration 97: Fourth Decennial International Conference on Mineral exploration (DMEC), pp. 249–260.
Gass, I.G., 1981. Pan-African (Upper Proterozoic) plate tectonics of the Arabian-Nubian Shield. In: Kroner, A. (Ed.), Precambrian Plate Tectonics. Elsevier, pp. 387–405.
Getaneh, A., Saxena, G., 1984. A review of Ethiopian lignite occurrences, prospects and possibilities [J]. Energy Explor. Exploit. 3, 35–132.
Ghebretensae, G.F., Yao, H.-Z., Zhao, K., Zhao, J.-H., 2019. Petrogenesis and tectonic implications of the Neoproterozoic adakitic and A-type granitoids in the southern Arabian-Nubian shield. Arabian J. Geosci. 12 (14), 428. https://doi.org/10.1007/s12517-019-4575-x.
Goossens, P.J., 2000. Chronique africaine: Egypte, Lybie, Erythree, Ethiopie, Somalie, Djibouti. Les Techniques de l'Industrie Minerale, suppl. au no. 8.
Hamrla, M., 1978. The Massive sulphides and magnetite deposits of northern Ethiopia [J]. Geologija 21, 255–310.
HU, Jia-ming, YI, Chao, 2017. Determination of CaO and MgO in cement limestone by inductively coupled plasma atomic emission spectrometry[J]. Anal. Test. Technol. Instrum. 23 (4), 245–249. https://doi.org/10.16495/j.1006-3757.2017.04.006.
Johnson, P.R., Andresen, A., Collins, A.S., Fowler, A.R., Fritz, H., Ghebreab, W., Kusky, T., Stern, R.J., 2011. Late Cryogenian-Ediacaran history of the Arabian-Nubian shield: a review of depositional, plutonic, structural, and tectonic events in the closing stages of the northern East African Orogen. J. Afr. Earth Sci. 61, 167–232.
Johnson, C.C., Breward, N., Ander, E.L., Ault, L., 2005. G-BASE: baseline geochemical mapping of Great Britain and Northern Ireland. Geochem. Explor. Environ. Anal. 5, 347–357.
Johnson, C.C., Flight, D.M., Ander, E.L., et al., 2018. The collection of drainage samples for environmental analyses from active stream channels. Environmental geochemistry. Elsevier, pp. 47–77.
Kazmin, V., 1971. Precambrian of ethiopia. Nat. Phys. Sci. Lond. 280, 176–177.
Kazmin, V., 1975. The precambrian of ethiopia and some aspects of the geology of the mozambique belt. Bull. Geophys. Obs. Addis Ababa Univ. 15, 27–43.
Kazmin, V., Shifrau, A., Balcha, T., 1978. The Ethiopian basement; Stratigraphy and possible manne of evolution. Geol. Rundsch. 67 (2), 531–546.

Key, R.M., De Waele, B., Liyungu, A.K., 2004. A multi-element baseline geochemical database from the western extension of the Central African Copperbelt in north western Zambia. Trans. Inst. Min. Metall. B Appl. Earth Sci. 113, 205–226.
KHAN, Junaid, Yao Hua-Zhou, Jun-Hong Zhao, Qi-Wei Li, Wen-Shuai Xiang, Jun-Sheng Jiang,TAHIR Asma, 2022. Petrogenesis and tectonic implications of the Tertiary Choke shield basalt and Continental flood basalt from the Central Ethiopian plateau. journal of Earth sciences. Submitted for publication.
Kirkwood, C., Everett, P., Ferreira, A., Lister, B., 2016. Stream sediment geochemistry as a tool for enhancing geological understanding: an overview of new data from southwest England. J. Geochem. Explor. 163, 28–40.
Knot, W., Abera, S., 1983. Report on diatomite and bentonite clay on Gidicho Island, Lake Abaya. EIGS, Addis Ababa. Unpublished report, 23 p.
Kroner, A., 1985. Ophiolites and the evolution of tectonic boundaries in the Late Proterozoic Arabian-Nubian shield of north-east Africa and Arabia. Precamb. Res. 27, 277–300.
Kroner, A., Linnebacher, P., Stern, R.J., Reischmann, T., Manton, W., Hussein, I.M., 1991. Evolution of Pan-African island arc assemblages in the southern Red Sea Hills, Sudan, and in southwestern Arabia as exemplified by geochemistry and geochronology. Precamb. Res. 53, 99–118.
Kuznetsova, A.I., Zarubina, O.V., Sklyarova, O.A., 2007. Determination of trace elements (Ag, B, Ge, Mo, Sn, W, Tl) in reference samples of soils and bottom sediments by atomic emission spectrometry: a traceability and fitness-for-purpose study. Geostand Geoanalyt. Res. 31 (3), 251–259.
Lapworth, D.J., Knights, K.V., Key, R.M., Johnson, C.C., Ayoade, E., Adekanmi, M.A., Arisekola, T.M., Okunlola, O.A., Backman, B., Eklund, M., Everett, P.A., Lister, R.T., Ridgway, J., Watts, M.J., Kemp, S.J., Pitfield, P.E.J., 2012. Geochemical mapping using stream sediments in west-central Nigeria: Implications for environmental studies and mineral exploration in West Africa. Appl. Geochem. 27 (6) https://doi.org/10.1016/j.apgeochem.2012.02.023.
Mengistu, T., 1987. Exploration on bentoniticclay in Hararghe and Wollo administrative regions. EIGS, Addis Ababa. Unpublished report, 12 p.
Mengistu, T., Fentaw, H.M., 1994. Nature and economic potential of Kombelcha (Ethiopia) kaolin. Conf., Karachi 26, 29.
Mengistu, T., Fentaw, H.M., 1993. Kaolin resources of weathered granites near Kombelcha, eastern Hararghe. EIGS, Addis Ababa. Unpublished report, 49 p.
Mengistu, T., Fentaw, H.M., 2000. The industrial mineral and rock resource potential of Ethiopia. Chron. Rech. Min. 540, 33–40.
Mogessie, A., Belete, K.H., 2000. Platinum and gold mineralization in the Yubdo mafic-ultramafic rocks, western Ethiopia: historical perspective and some new results. Chron. Rech. Min. 540, 53–62.
Nforba, M.T., Egbenchung, K.A., Berinyuy, N.L., Mimba, M.E., Tangko, E.T., Nono, G.D. K., 2020. Statistical evaluation of stream sediment geochemical data from Tchangue-Bikoui drainage system, Southern Cameroon: a regional perspective. Geol. Ecol. Landsc. https://doi.org/10.1080/24749508.2020.1728023.
Plant, J.A., Smith, D., Smith, B., Williams, L., 2001. Environmental geochemistry at the global scale. Appl. Geochem. 16, 1291–1308.
Standards Press of China (SPC), 2004.China Geological Survey. Technical requirements for strategic minieral exploration (on trial) . DD2004-04 Beijing.
Ranasinghe, P.N., Fernando, G.W.A.R., Dissanayake, C.B., Rupasinghe, M.S., Witter, D.L., 2009. Statistical evaluation of stream sediment geochemistry in interpreting the river catchment of high grade metamorphic terrains. J. Geochem. Explor. 103, 97–114.
Reimann, C., Äyräs, M., Chekushin, V., Bogatyrev, I., Boyd, R., de Caaritat, P., Dutter, R., Finne, T.E., Halleraker, J.H., Jager, Ø, Kashulina, G., Lehto, O., Niskavaara, H., Pavlov, V., Räisänen, M.L., Strand, T., Volden, T., 1998. Environmental Geochemical Atlas of the Central Barents Region. Geological Survey of Norway.
Ren, T.X., Yin, B.C., Liu, R.Y., et al., 1993.The Background Values of 39 Elements in Stream Sediments of China.In:Organizing Committee of 5th National Exploration Geochemistry Symposium, ed., Abstracts of 5th National Exploration Geochemistry Symposium.Geological Publishing House, Beijing, 126-127 (in Chinese).
Rice, K.C., 1999. Trace-element concentrations in streambed sediment across the conterminous United States. Environ. Sci. Technol. 33, 2499–2504.
Ridgway, J., Johnson, C.C., Lapworth, D.J., Key, R.M., 2009. Field procedures manual for the geochemical mapping of Nigeria. Nigerian Geochemical Mapping Technical Assistance Project. Brit. Geol. Surv. Commissioned, Report, CR/09/021.
Sabov, Y.V., Mohammed, S., Walle, H., 1983. Bombowha kaolin and Kenticha feldspar, quartz deposits. EIGS, Addis Ababa. Unpublished report, 184p.
Salminen, R., (Chief-editor), Batista, M.J., Bidovec, M., Demetriades, A., De Vivo, B., De Vos, W., Duris, M., Gilucis, A., Gregorauskiene, V., Halamic, J., Heitzmann, P., Lima, A., Jordan, G., Klaver, G., Klein, P., Lis J., Locutura, J., Marsina, K., Mazreku, A., O'Connor, P.J., Olsson, S.Å., Ottesen, R.-T., Petersell, V., Plant, J.A., Reeder, S., Salpeteur, I., Sandström, H., Siewers, U., Steenfelt, A., Tarvainen, T., , 2005. Geochemical Atlas of Europe. Part 1—Background Information, Methodology and Maps.
Sánchez-Rodas, D., Corns, W. T., Chen, B., Stockwell, P. B., 2010. Atomic Fluorescence Spectrometry: a suitable detection technique in speciation studies for arsenic, selenium, antimony and mercury. 25(7), 933-0. doi:10.1039/b917755h.
Selassie, M.G., Reimold, W.U., 2000. A review of the metallic mineral resource potential of Ethiopia. Chronique de la recherche minière 540, 11–32.
Shackleton, R.M., 1986. Precambrian collision tectonics in Africa. Geol. SOC. Sp. Publ. No. 19, pp. 329-349.
Shackleton, R.M., 1994. Review of Late Proterozoic sutures, ophiolitic melanges and tectonics of eastern Egypt and north-east Sudan. Geol. Rundsch 83, 537–546.
Stern, R.J., 1994. Arc assembly and continent collision in the Neoproterozoic East African Orogen: implication for the consolidation of Gondwanaland[J]. Ann. Rev. Earth Planet. Sci. 1994 (23), 289–310.
Stern, R.J., Avigad, D., Miller, N.R., Beyth, M., 2005. Evidence for the snowball earth hypothesis in the Arabian-Nubian shield and the East African Orogen. J. Afr. Earth Sci. 44, 1–20. https://doi.org/10.1016/j.jafrearsci.2005.10.003.
Tadesse, S., 2000. Origin of the Lega Dembi primary gold deposit, Adola gold field, southern Ethiopia. Afr. Geosci. Rev. 7 (1), 83–90.
Tadesse, S., 2001. Epithermal gold occurrences in the Lakes District of the Main Ethiopian Rift: Discovery of a metallogenic province. SINET: Ethiop. J. Sci. 24 (1), 69–91.
Tadesse, S., 2004. Genesis of the shear zone-related gold vein mineralization of the lega dembi gold deposit, adola gold field, Southern Ethiopia [J]. Gond. Res. 7 (2), 481–488.
Tadesse, S., Milesi, J.P., Deschamps, Y., 2003. Geology and mineral potential of Ethiopia: a note on geology and mineral map of Ethiopia. Journal of African Earth Sciences 36 (4), 273–313.
Thomas, J.M., William, R.G., 1997. Inductively coupled plasma – Atomic emission spectrometry. Chem. Educator 2 (1), 1–19. https://doi.org/10.1007/s00897970103a.
Whitehead, A. B., Heady, H. H., 1970. Fire-Assay Emission Spectrographic Method for Platinum, Palladium, Rhodium, and Gold. as/24/2/as-24-2-225.pdf, 24(2), 225–228. doi:10.1366/000370270774371868.
Williams, F. M., 2016. Understanding Ethiopia. Wolfgang Eder AV. Springer International Publishing Australia org/10.1007/978-3-319-02180-5.
Woldemichael, B.W., Kimura, J.-I., Dunkley, D.J., Tani, K., Ohira, H., 2009. SHRIMP U-Pb zircon geochronology and Sr–Nd isotopic systematic of the Neoproterozoic Ghimbi-Nedjo mafic to intermediate intrusions of Western Ethiopia: a record of passive margin magmatism at 855 Ma? Int. J. Earth Sci. (Geol Rundsch) 99, 1773–1790. https://doi.org/10.1007/s00531-009-0481-x.
Xie, X.J., Ye, J.Y., Yan, M.C., Zhou, G.H., 2003. New proficiency test for the analytical laboratories involved in the environmental geochemical mapping. Geol. Bull. China 22, 1–11. In Chinese.
Xiong, Chuan Xin; Liu, Ya Rong; Gu, Juan Ping, 2011. Rapid Determination of As, Sb, Bi and Hg in Gold Ore Samples by AFS with L-Cysteine as a Prereducer. Advanced Materials Research, 304, 328–333. doi:10.4028/www.scientific.net/AMR.304.328.
Yao, Wensheng, Xie, Xuejing Wang, Xueqiu, 2011. Comparison of results analyzed by Chinese and European laboratories for FOREGS geochemical baselines mapping samples. Geoscience Frontiers 2 (2), 247–259. https://doi.org/10.1016/j.gsf.2011.03.002.
Ye, J.Y., 2002. Quality monitoring and quality control of samples analysis in regional geochemical survey. Geophys. Geochem. Explor. 26, 6–11. In Chinese.
Ye, J.Y., Yao, L., 2004. Discussion of quality control method for the analysis of samples in regional geochemical survey. Rock Mineral Anal. 23, 137–142. In Chinese.
Young, S.M., Pitawala, A., Ishiga, H., 2013. Geochemical characteristics of stream sediments, sediment fractions, soils, and basement rocks from the Mahaweli River and its catchment, Sri Lanka. Chem. Erde 73, 357–371.